

Cite this: *Chem. Soc. Rev.*, 2023, 52, 5684

## DNA-mediated regioselective encoding of colloids for programmable self-assembly

Longjiang Ding,<sup>†[a](#)</sup> Xiaoliang Chen,<sup>†[a](#)</sup> Wenhe Ma,<sup>a</sup> Jiang Li,<sup>ID [b](#)</sup> Xiaoguo Liu,<sup>ID [a](#)</sup> Chunhai Fan <sup>ID [a](#)</sup> and Guangbao Yao <sup>ID [a](#) \*</sup>

How far we can push chemical self-assembly is one of the most important scientific questions of the century. Colloidal self-assembly is a bottom-up technique for the rational design of functional materials with desirable collective properties. Due to the programmability of DNA base pairing, surface modification of colloidal particles with DNA has become fundamental for programmable material self-assembly. However, there remains an ever-lasting demand for surface regioselective encoding to realize assemblies that require specific, directional, and orthogonal interactions. Recent advances in surface chemistry have enabled regioselective control over the formation of DNA bonds on the particle surface. In particular, the structural DNA nanotechnology provides a simple yet powerful design strategy with unique regioselective addressability, bringing the complexity of colloidal self-assembly to an unprecedented level. In this review, we summarize the state-of-art advances in DNA-mediated regioselective surface encoding of colloids, with a focus on how the regioselective encoding is introduced and how the regioselective DNA recognition plays a crucial role in the self-assembly of colloidal structures. This review highlights the advantages of DNA-based regioselective modification in improving the complexity of colloidal assembly, and outlines the challenges and opportunities for the construction of more complex architectures with tailored functionalities.

Received 13th December 2022

DOI: 10.1039/d2cs00845a

rsc.li/chem-soc-rev

<sup>a</sup> School of Chemistry and Chemical Engineering, Frontiers Science Center for Transformative Molecules and National Center for Translational Medicine, Shanghai Jiao Tong University, Shanghai 200240, China.

E-mail: yaoguangbao@sjtu.edu.cn

<sup>b</sup> Institute of Materiobiology, Department of Chemistry, College of Science, Shanghai University, Shanghai 200444, China

† These authors contributed equally.



Longjiang Ding

Longjiang Ding received his PhD degree from Fudan University in 2020. He then worked as a postdoctoral researcher at the School of Chemistry and Chemical Engineering, Shanghai Jiao Tong University (2020–2022), and 2nd Physics Institute, University of Stuttgart (2023–present). His research interests are mainly focused on DNA nanotechnology, optical sensors and colloidal assembly.



Xiaoliang Chen

### 1. Introduction

Colloids are dispersed particles that range in size from several nanometers to several micrometers. Colloidal particles can be made from almost any material, including metals, polymers, semiconductors, and oxides.<sup>1</sup> Colloidal self-assembly has been proposed as an ideal method for bottom-up programming of functional materials.<sup>1,2</sup> The resulting ensembles have synergistic optical, electronic, and magnetic properties that differ

Xiaoliang Chen received his PhD degree from the Shanghai Institute of Applied Physics, Chinese Academy of Sciences (CAS), in 2020. He then worked as a postdoctoral researcher at the School of Chemistry and Chemical Engineering, Shanghai Jiao Tong University. His research interests are mainly focused on DNA nanotechnology and colloidal assembly.

from those of individual particles and their bulk counterparts.<sup>1–4</sup> As a result, self-assembly of colloids into superstructures has significant potential in fields including plasmonic,<sup>5</sup> photonic,<sup>6</sup> catalysis<sup>7</sup> and sensing.<sup>8</sup> Furthermore, colloidal assembly is an excellent model system for studying atomic phase transitions in nature. These colloids can form crystals and other phases of matter seen in atomic and molecular systems through self-assembly. Unlike atoms or molecules, these particles are large enough that the microscopic mechanism of the phase transition can be directly observed under an optical<sup>9</sup> or electron microscope.<sup>10</sup>

In general, the self-assembly of colloids is typically governed by their sizes, shapes, compositions and surface features. The interactions between particles include electrostatic interactions, van der Waals forces, hydrogen bonding, and so on. The emergence of colloidal platforms with molecular recognition, along with the ability to decorate particle surfaces with recognition motifs, has facilitated the formation of colloidal assemblies through directional interactions and shape

recognition.<sup>11</sup> Beyond its role as a carrier of genetic information, deoxyribonucleic acid (DNA) is an ideal ligand with programmable interactions that can direct the assembly of colloidal particles into finite or extended structures.<sup>12–14</sup> Compared with other ligands, DNA molecules have several advantages, including predictable Watson–Crick base-pairing interactions, programmable sequences and controllable lengths.<sup>11,15</sup> With the maturing of chemical and biological synthesis technology, researchers can now obtain DNA molecules with a designed sequence and a variety of chemical linkers (*e.g.*, thiol, amino, biotin, azide and so on). Therefore, DNA molecules can be decorated on the surface of various particles using coupling chemistry and click chemistry, such as Au–S interaction for gold nanomaterials,<sup>16</sup> ligand–receptor binding,<sup>17</sup> physical grafting,<sup>18</sup> and covalent attachment<sup>19,20</sup> for polymer or silica particles. Moreover, a major trait of using DNA for colloidal assembly is the ability to control the interparticle distance. This is due to the programmability of DNA through sequence-specific hybridization and the rigidity of the



**Wenhe Ma**

Wenhe Ma obtained his bachelor's degree in chemistry and biology from Xi'an Jiaotong University, in 2021. He is now a PhD student at Shanghai Jiao Tong University, majoring in chemistry under the supervision of Prof. Chunhai Fan. His research interests are DNA nanotechnology, colloidal self-assembly and DNA-based data storage.



**Jiang Li**

Jiang Li obtained his BS and PhD degree from Sichuan University in 2003 and 2009, and joined the faculty at Shanghai Institute of Applied Physics, Chinese Academy of Sciences (CAS) (2009–2018). Then he joined the Bioimaging Center, Zhangjiang Laboratory, Shanghai Advanced Research Institute, CAS (2018–2023). Now, he is a professor at the Institute of Materiobiology, Department of Chemistry, College of Science, Shanghai University. His research interests include developing DNA nanotechnology-empowered nanoprobe and cell imaging strategies.



**Xiaoguo Liu**

Xiaoguo Liu obtained his BS from Jilin University in 2008 and his PhD from Shanghai Institute of Ceramics, Chinese Academy of Sciences (CAS), in 2013. From 2013 to 2018, he was a postdoctoral fellow and then an assistant professor at Shanghai Institute of Applied Physics. In 2018, he assumed a tenure track associate professor position at Shanghai Jiao Tong University. His research interests include inorganic biomaterials, biomimetic mineralization, DNA nanotechnology, and synchrotron SAXS.



**Chunhai Fan**

Chunhai Fan is a K. C. Wong chair professor at Shanghai Jiao Tong University (SJTU) and a member of the Chinese Academy of Sciences (CAS). Before joining SJTU, he was a CAS distinguished professor at the Shanghai Institute of Applied Physics. He is a fellow of the Royal Society of Chemistry (FRSC), and an elected fellow of the International Society of Electrochemistry (ISE) and American Association for the Advancement of Science (AAAS). His research interests include DNA nanotechnology, DNA data storage, and computing.

double-stranded structure, which has a persistence length of about 50 nm.<sup>12</sup> Furthermore, the use of three-way or four-way junctions can even result in longer persistence lengths. In addition, structural DNA nanotechnology enables DNA to form various geometries and motifs beyond the standard double helix, and then assemble into 1D, 2D, and 3D structures.<sup>21</sup>

DNA-mediated colloidal assembly originated from two pioneering papers published back-to-back in *Nature* in 1996. In one paper, Mirkin and colleagues used Au–S chemistry to uniformly modify spherical colloidal gold nanoparticles (AuNPs, about 13 nm in diameter) with multiple DNA strands.<sup>16</sup> In another paper, Alivisatos and colleagues showed that small (1–2 nm) AuNPs can be functionalized with as few as one DNA strand per particle.<sup>22</sup> The isotropic DNA-particle conjugate developed by Mirkin was named spherical nucleic acid (SNA) because of the multiple nucleic acid strands wrapped around the spherical core particle.<sup>23</sup> Over the past few decades, SNAs have been intensively investigated for their ability to form particle aggregates and superlattices with distinct crystalline symmetries. In colloidal crystal engineering with DNA, these isotropic modified nanoparticles are generally considered as “programmable atom equivalents” (PAEs). PAEs with fixed positions and coordination numbers are contained within superlattices similar to atoms in metals or ionic solids.<sup>24</sup>

Once a single distinct region on a particle could be deliberately functionalized with programmable DNA bonds, the stoichiometry, spatial arrangement and relative orientation of an individual colloid in assemblies could be precisely controlled. Importantly, regioselective surface encoding with DNA is crucial for fields where specific, directional, and orthogonal recognition interactions are required.<sup>24–33</sup> Nevertheless, achieving regioselective modification on the surface of such a tiny colloid remains elusive. The main barrier is to alter the isotropic chemical environment on particle surfaces, especially for homogeneous spherical particles. Alivisatos and coworkers sought to break the symmetry of particles by functionalizing the AuNPs with as few as one DNA “codon” (a single-stranded DNA of defined length and sequences) per particle.<sup>22</sup> Regioselective surface modification with DNA was first introduced, allowing the assembly of finite “nanocrystal molecules” rather



**Guangbao Yao**

*Guangbao Yao obtained his BS and PhD degree from Sichuan University in 2010 and 2015. He was a postdoctoral fellow at Shanghai Institute of Applied Physics, Chinese Academy of Sciences (CAS) (2015–2017) and at Arizona State University (2017–2020). He is currently an associate professor at Shanghai Jiao Tong University. His research interests include DNA nanotechnology, colloidal assembly and nanoelectronics.*

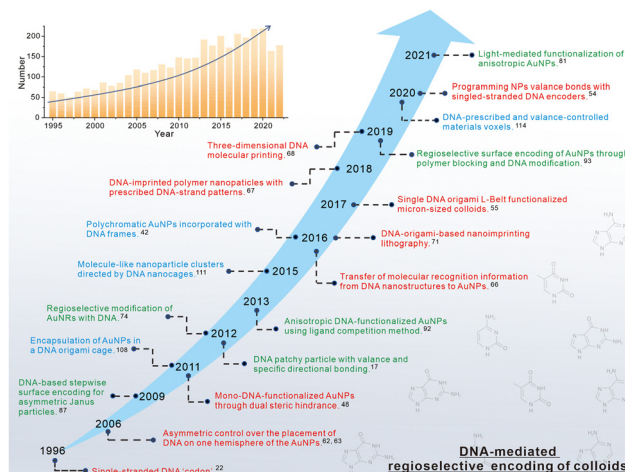


**Fig. 1** The timeline of some significant events in DNA-mediated regioselective encoding of colloids. Inset: Count of paper result by searching “(colloid OR particle) AND assembly AND DNA” in Pubmed. The color coding used, red, green, and blue, represents the strategies of number-defined DNA molecules, DNA patches, and DNA origami shells, respectively.

than bulk structures. The amount of DNA on a particle determines its coordination number, which is analogous to the valence of an atom in a molecule system.<sup>34–38</sup> Since then, a variety of DNA-mediated regioselective surface encoding approaches have been developed to explore novel assembled structures both in experiment and simulation (Fig. 1).<sup>13,39,40</sup> Especially with the considerable development of structural DNA nanotechnology, DNA nanostructure-based regioselective surface encoding has attracted increasing attention in colloidal assembly.

Fig. 2 illustrates three typical strategies for regioselective encoding of colloids with number-defined DNA molecules, DNA patches, and DNA origami shells. The strategy of DNA

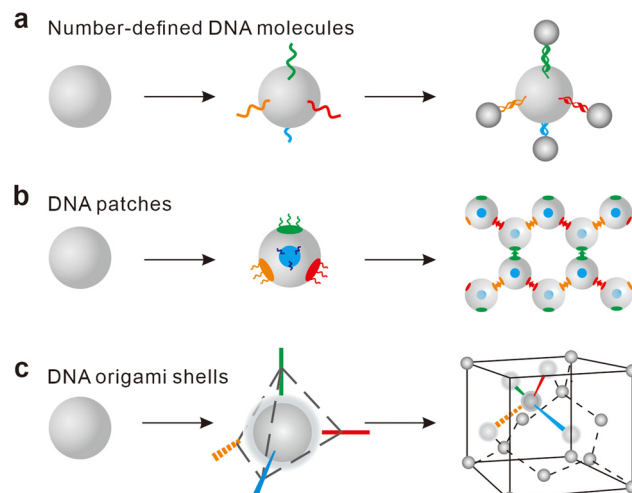


**Fig. 2** Three typical DNA-mediated regioselective encoding strategies for programmable colloidal self-assembly, including (a) number-defined DNA molecules, (b) DNA patches and (c) DNA origami shells.

molecules with a pre-determined number has evolved from the Alivisatos' pioneering concept of DNA "codon", which relies on controlling the number of DNA strands on each particle. Each encoding region on the particle surface has only one DNA domain, or its equivalent. This strategy provides specific bonding interactions to prepare atom-like particles with  $n$ -valence that can be used to assemble low-coordination colloidal molecules (Fig. 2a). Another strategy is to decorate the surface of colloidal particles with "sticky patches" made of multiple DNA strands.<sup>2,41</sup> The patches on the colloidal particles provide directionality, whereas multiple sticky DNA strands on each patch provide specificity and stronger bonding interactions. As a result, this strategy of DNA patches enables the production of long-range and higher-ordered colloidal assemblies in addition to the colloidal analogues of atoms (Fig. 2b). With the DNA nanotechnology boom,<sup>21</sup> colloidal nanoparticles can be encapsulated in various DNA origami structures. The position and number of patches are defined by the DNA origami shells.<sup>42</sup> This strategy allows the construction of more complex two- and three-dimensional assemblies by providing specific, directional, and orthogonal bond interactions (Fig. 2c). The seminal advances of each strategy have been demonstrated in Fig. 1. The color coding used, with red, green, and blue, represents the regioselective encoding strategies of number-defined DNA molecules, DNA patches, and DNA origami shells, respectively.

This review details the progress of DNA-mediated regioselective surface encoding of colloids. We summarize the established experimental strategies for regioselective modification of colloids with DNA, followed by a discussion of the most representative assemblies based on regioselective DNA-encoded particles. In the end, we elucidate perspectives on the challenges and opportunities for the formation of more complex architectures with tailored functionalities.

## 2. Regioselective encoding with number-defined DNA molecules

### 2.1 Single DNA molecule

In comparison with DNA multiple-modification, attaching a single copy of single-stranded DNA (ssDNA) to the surface of a spherical colloid is the most straightforward method to achieve regioselective surface functionalization.<sup>22,43–46</sup> Due to the presence of multiple attaching sites on the particle surface, chemically attaching ssDNA to colloids results in products with valences that follow a Poisson distribution, where the desired products with specific valence are always obtained alongside unconjugated and multivalent byproducts.<sup>47</sup> Consequently, these approaches typically involve a purification step to isolate particles bearing discrete numbers of DNA strands. Steric hindrance<sup>48</sup> and surface-based masking strategies that block part of the nanoparticle surface<sup>49</sup> improved the yield of monovalent products. Jun and colleagues used a steric-exclusion strategy to limit the maximum valency of products by sterically excluding a large fraction of the particle surface from further reactions (Fig. 3a).<sup>50</sup> The phosphorothioate DNA (ptDNA) wraps each CdSe:ZnS quantum dot (QD, with a diameter of ~10 nm) in a single synthetic step. The irreversibly formed monovalent products could prevent the binding of a second DNA molecule, resulting in the formation of monovalent QDs with a high yield (>95%). A similar steric technique was used to create monovalent AuNPs with a long sticky poly adenine (polyA) domain.<sup>51</sup> Zimmerman and colleagues developed a bottom-up polymer-based method for the synthesis of monovalent DNA-nanoparticle conjugates.<sup>52</sup> This method allows for the effective conjugation of a single DNA strand to each polymeric organic nanoparticle (ONP, with a diameter of *ca.* 15–20 nm). The monovalency was controlled by the parent linear block

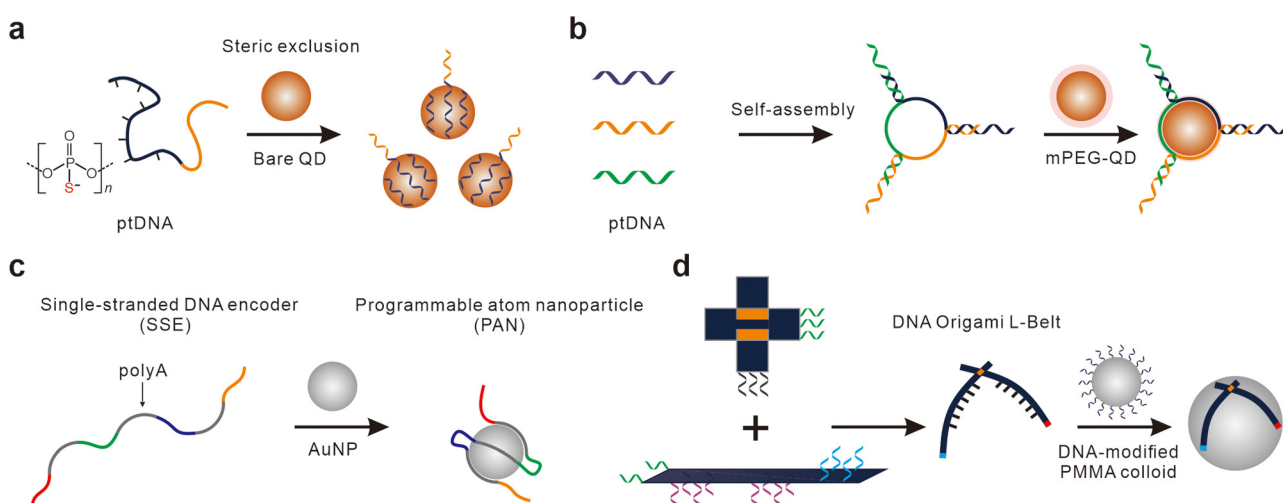


**Fig. 3** Single DNA molecule. (a) Schematic illustration depicting the formation of monovalent QDs (~10 nm) with ptDNA molecules. A single ptDNA was wrapped around the nanoparticle surface, preventing the adsorption of a second strand due to steric exclusion.<sup>50</sup> (b) Schematic illustration of valence-engineered QDs (~4 nm) with multi-armed DNA scaffolds.<sup>53</sup> (c) General design principle for SSE based noncovalent synthesis of PANs using AuNPs (5 nm, 10 nm, 15 nm and 20 nm). The SSE is composed of alternating polyA and non-polyA domains.<sup>54</sup> (d) Schematic illustration of the synthesis of multivalent colloidal microparticles (0.71  $\mu\text{m}$ ) with a single DNA origami L-Belt-based encoder.<sup>55</sup>

copolymers of ONPs with only one reactive group for DNA conjugation at the chain-end.

Although significant progress has been made in the formation of monovalent particles with a quantitative yield, achieving quantitative control of multivalent particles remains challenging. Divalent nanoparticles were accomplished using the reactivity of the polar singularities for a replacement reaction, where two ssDNA were placed on a particle in a geometrically controlled manner at diametrically opposed positions.<sup>56</sup> Fan and colleagues presented a DNA-programmed strategy for valence engineering of CdSe:ZnS QDs with high modularity and yield by combining the steric exclusion effect with electrostatic repulsion.<sup>53</sup> As shown in Fig. 3b, the neutral mPEG reduced the negative surface charge and favored the subsequent DNA approach, whereas an appropriately sized ptDNA molecule wrapped the QD (with the size of approximately 4 nm) and prevented the reaction of a second strand due to steric exclusion. By employing a series of programmable DNA scaffolds, QDs of customized valency were obtained in a single step without purification. The formation yield of monovalent and divalent QDs is higher than 95%, while for trivalent and tetravalent QDs, it is about 80–85%.

Furthermore, depending on the highly specific consecutive gold–adenine coordination, the AuNPs (5 nm, 10 nm, 15 nm and 20 nm) with programmable valence bonds were constructed using polyA-containing single-stranded DNA encoders (SSE) (Fig. 3c).<sup>54</sup> Previously, it has been demonstrated that the relative spatial arrangement of DNA strands anchored on the particle surface could be controlled by the length of polyA units.<sup>57</sup> In this study, the single-stranded encoder was reliably patterned by alternating sticky polyA domains and nonstick bonding domains, forming the desired three-dimensional (3D) spatial organization on the particle surface.<sup>54</sup> The programmable atom-like nanoparticles (PANs) with a defined number of valence-mimicking hybridizable bonds were synthesized by programming the order, length, and sequence of each segment of strand. Using the 10 nm sized AuNPs as an example, the yields of monovalent, divalent, trivalent and tetravalent PAN were estimated to be 45%, 48%, 60% and 82%, respectively. This design strategy is applicable to AuNPs with various sizes, although the yields may vary. For instance, using the same SSE sequences, the tetravalent PANs formed from AuNPs with distinct sizes (5 nm, 15 nm, and 20 nm) have yields of 88%, 38%, and 30%, respectively. In particular, the sequence of non-polyA domains encoded the orthogonality, while tuning the length of the polyA domain enabled control over the bond angles. This has been verified through TEM images, all-atomistic molecular dynamics (MD) simulations and cryogenic electron microscopy (cryo-EM) images. A large portion of the colloidal molecules resulting from SSEs with polyA lengths of A20 presented bond angles between 60° and 90°. For A30, the angles were predominantly distributed between 90° and 120°. Lastly, for A40, the distribution was approximately 120° to 150°, which corresponds to the theoretical bond angles of about 78°, 117°, and 156°, respectively.

This type of single polyA-based chimeric ssDNA molecule can also be used to control the surface chemistry of QDs.<sup>58</sup> Additionally, this single ssDNA-mediated encoding strategy has been used to modify the surface of ultra-small gold nanoclusters, and the hydrodynamic size increased from ~1 to ~2 nm after single DNA molecular modification.<sup>59</sup>

A conceptual leap in the strategy of single DNA molecules was made in 2017 when the multivalent principle was extended from the nanometric scale to micron regime by a single DNA origami molecule.<sup>55</sup> The employed DNA origami was folded into a nanostructure arbitrarily using multiple short DNA staple strands with a long DNA scaffold strand.<sup>21</sup> In this work, Chaikin and co-workers designed an elongated, belt-like DNA origami with a high aspect ratio (580 nm long, 10 nm wide, 2 nm thick). The belt-like DNA origami spanned a sizable arc-length on the surface of a 0.71 μm diameter polymethyl methacrylate (PMMA) particle, which is equivalent to the single ssDNA-based encoders for nanoparticles. The length and mechanical bending rigidity of the origami have been tailored to trace a geodesic on the curved surface of a colloid. Persistence lengths perpendicular to the flat face and parallel to the face along the width were designed to be 200 nm and 3200 nm respectively, ensuring the origami belt lay straight on the colloidal surface. As shown in Fig. 3d, the adhesive sticky ends below the surface worked as the sticky patches complementary to the colloid. The top-side multiple DNA sequences that pointed away from the central particle were used for the construction of multivalent bonds with prescribed binding angles. More recently, another semirigid DNA origami structure has also been anchored to a colloidal bead with as few as one origami molecule per particle.<sup>60</sup>

## 2.2 Patterned DNA molecules

To enable a higher level of control over the assembled structures, the creation of colloids that possess spatially addressable DNA bonds has received considerable attention.<sup>61</sup> Transferring a defined DNA pattern from the template to colloid is an efficient method for achieving spatially addressable DNA bonds on the colloidal surface. The utilization of larger particles as templates to transfer DNA to small particles has been demonstrated to realize the asymmetric spatial distribution of DNA bonds on colloidal surfaces. Mirkin and co-workers first demonstrated two DNA transfer strategies in 2006.<sup>62,63</sup> Both methods relied on the difference in melting temperatures of different DNA bonds. Following the capture of new DNA linkers at the interface of two particles, heating separated small nanoparticles with linker strands form larger particles. Small AuNPs simply acquired linker strands and were released from silica particles in one case (Fig. 4a).<sup>62</sup> In the other case, the DNA strands of the small AuNPs were enzymatically ligated to short linker strands on magnetic microparticles (2.8 μm diameter) before being released (Fig. 4b).<sup>63</sup>

Although the transfer method confers significant spatial regioselectivity on isotropic particles, it is more difficult to place DNA strands with different sequences and patterns on particles. Suzuki *et al.* immobilized two different thiolated DNA

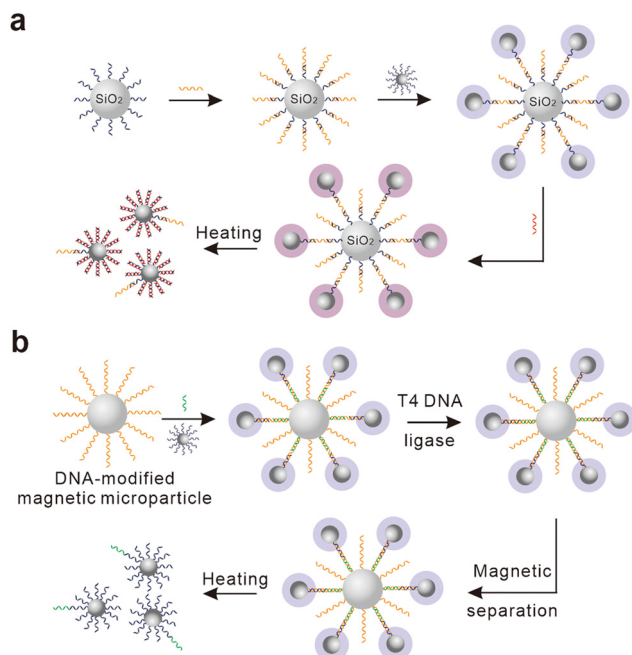


**Fig. 4** Asymmetric DNA molecules transferred from particle templates. (a) Transferring DNA molecules from DNA-modified silica particles to AuNPs.<sup>62</sup> (b) Transferring DNA molecules from DNA-modified magnetic particles (2.8  $\mu\text{m}$ ) to AuNPs using T4 DNA ligase as an assisting agent.<sup>63</sup>

strands in a specific arrangement on the surface of AuNPs.<sup>64</sup> The arrangement was defined using a linear DNA motif template.<sup>64,65</sup> They demonstrated that spatial information could be transferred from a geometrical DNA template to the particle surface. 3D DNA structures, which act as programmable parent templates for DNA transfer, provide nanoparticles with more precise and complex site-specific addressability. Sleiman and colleagues demonstrated the feasibility of this concept in 2016 by presenting the first example of molecular printing of multiple DNA strands from DNA nanoscaffolds.<sup>66</sup> Rather than permanently attaching to nanoparticles, the DNA nanostructures were used as reusable templates to transfer a discrete pattern of DNA strands to the nanoparticles in a single cycle. As shown in Fig. 5a, up to four distinct DNA strands placed on the face of a cubic DNA template with precise arrangement were attached to a 10 nm AuNP. Upon denaturation of the DNA prismatic cube, these patterned DNA strands were molecularly printed onto the particle surface, preserving the original spatial positions and molecular recognition information. In addition to the exogenous printing method, the Sleiman group have also printed a specific pattern of six unique strands directly from a DNA cube scaffold to a polymeric core inside the cage.<sup>67</sup> Huang and colleagues reported an endogenous printing process within a DNA icosahedron cage for 3D molecular printing.<sup>68</sup>

The above-mentioned molecular transfer examples pattern nanoparticles using soft and small DNA templates, which limit the pattern to a relatively small solid angle. DNA origami structures provide alternative rigid and large templates for DNA pattern transfer. Each staple strand acts as a recognition

site for anchoring nanoparticles with unparalleled precision and addressability.<sup>21</sup> Fan and colleagues developed DNA-origami-based nanoimprinting lithography by transferring a DNA pattern from two-dimensional (2D) DNA origami onto both 30 nm sized AuNPs<sup>71</sup> and gold nanorods (AuNRs, 10 nm  $\times$  39 nm).<sup>72</sup> Instead of breaking the DNA structures, the strand-displacement reactions were used to separate the particles from the parent origami templates. More recently, this method has been used to transfer DNA strands with predefined sequences and positions to the surface of gold nanocubes (AuNCs) with the edge length of  $47.5 \pm 2.5$  nm and vertex curvature radius of 8.42 nm (Fig. 5b).<sup>69</sup> As a result, nine-valent AuNCs were obtained by placing nine DNA strands at the vertices, edges, and face of the AuNCs. Given the rich variety of DNA origamis, this strategy can also be extended to three-dimensions, enabling the regioselective functionalization of arbitrary sites on AuNCs. Gang and colleagues developed a molecular stamping approach to pattern nanoparticles with predefined DNA molecules using rigid and coordinative DNA origami frames (Fig. 5c).<sup>70</sup> Using the 3D tetrahedral frame and 2D single-layer frame as the molecular stamping apparatuses, multiple types of DNA molecular “inks” have been transferred onto a nanoparticle surface in a designed pattern, providing anisotropic bonds with distinctive bond interactions. Overall, DNA molecule transfer and printing methods broaden the strategy of single-stranded DNA encoding, allowing a particle to be decorated with arbitrarily designed DNA patterns.

### 2.3 Programmable assembly of colloids with number-defined DNA molecules

The monovalent particles can be easily assembled into dimers by adding particles with complementary DNA bonds.<sup>22,43,51,73</sup> Using divalent AuNPs with ssDNA bonds at each diametrically opposed position, linear one-dimensional (1D) and lattice-like 2D AuNP arrays with defined distances were created.<sup>56</sup> The yields, lengths, and widths of these nanoparticle arrays are insufficient to provide well-defined superstructural materials. As a result, the majority of single-DNA encoded anisotropic colloids are being developed for the bottom-up construction of finite oligomeric nanostructures with atom-like precision. A representative example is to fabricate homogeneous QDs-QDs and heterogeneous QDs-AuNP clusters by assembling monovalent, divalent, trivalent, and tetravalent QDs with complementary QDs and AuNPs of different diameters.<sup>53</sup> One feature of the single-DNA encoder is that the DNA bond length and bond energy can be engineered for hierarchical assembly of multiparticle structures, leading to increased freedom in design.<sup>54,73</sup> Fan and colleagues created up to 32 different types of colloidal oligomers by combining 16 different PAN species (Fig. 3c), which could be further used for the hierarchical assembly of branched colloidal molecules with multi-scale complexity (Fig. 6a). In addition, other low-coordination colloidal assemblies with compositions, sizes, chirality, and linearity have also been patterned by programming the DNA bonds. More importantly, colloidal reactions and structural

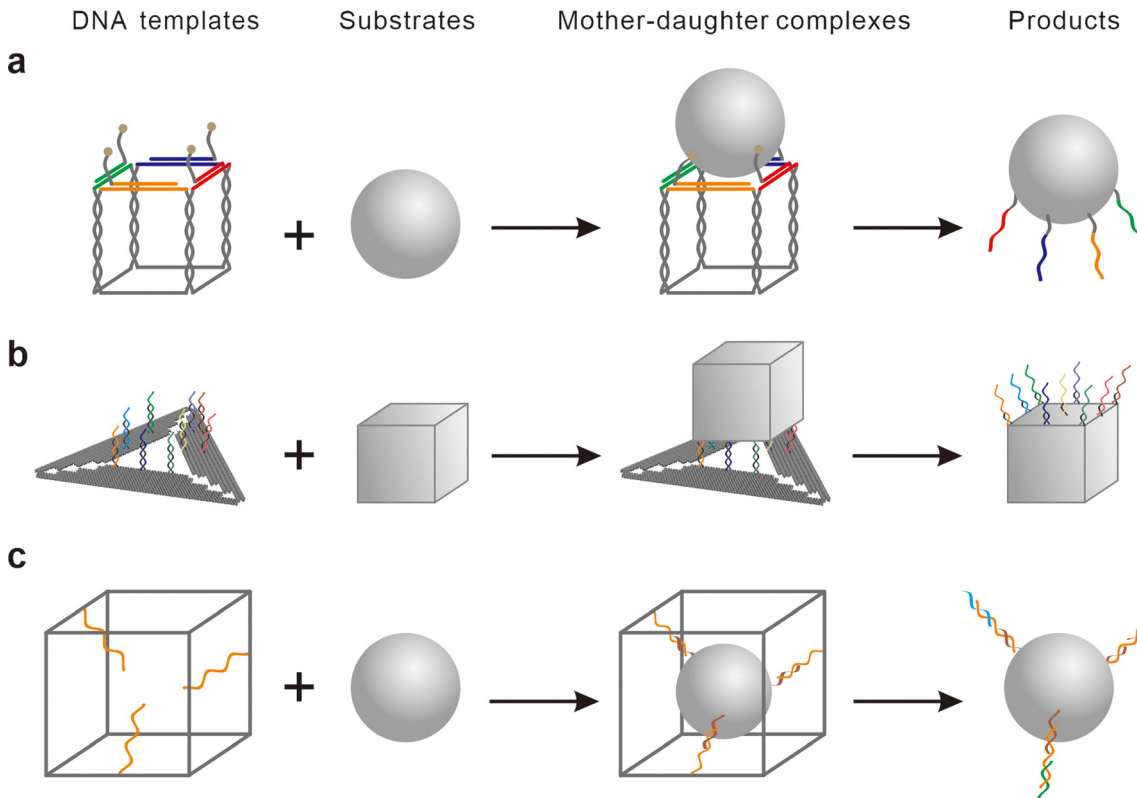


**Fig. 5** Patterned DNA molecules transferred from DNA nanoscaffolds. (a) An overview of the prismatic cube-based DNA printing strategy. The DNA prismatic cube hybridizes into AuNPs (10 nm) through Au–S bonds. When the DNA template is removed, the resulting products inherit the parent template's pattern and molecular recognition information.<sup>66</sup> (b) DNA origami-based nanoimprinting lithography for the fabrication of spatially controllable functionalized AuNCs (edge length:  $47.5 \pm 2.5$  nm, vertex curvature radius: 8.42 nm).<sup>69</sup> (c) Molecular stamping diagram using rigid and complementary DNA origami frames.<sup>70</sup>

rearrangement enable these assemblies to be dynamically reconfigurable.<sup>54</sup>

DNA molecular printing allows nanoparticles to have a similar nanoscale addressability to DNA nanostructures. DNA patterns with designed spatial information placed on the particle surface can thus enable autonomous assembly into geometrically controlled patterns.<sup>66,69,71,72</sup> As shown in Fig. 6b, the desired cluster structures (T1–T4) were generated using imprinted DNA bonds as the anchoring points (Fig. 5a). The interparticle distances matched the expected values for T1 and T2.<sup>66</sup> Furthermore, the nanoparticles modified using the 3D molecular stamping strategy can be assembled into specified cluster configurations with 360° spatial control.<sup>68,70</sup>

The typical M13-based 2D origami molecule has an area smaller than 90 nm by 90 nm and covers less than 0.3% of the surface of a 1 μm diameter spherical microparticle. As a result, DNA origami is not naturally commensurate with micron-sized colloids. However, the expanded DNA origami shown in Fig. 3d serves as a regioselective encoder for colloids that are significantly large in size (0.71 μm diameter microparticles are used here). Aside from overcoming the limitation that DNA nanostructures cannot completely cover micrometer-sized colloids, this custom-designed single DNA origami-based encoder provides rigidity and directionality for colloidal assembly. From

the wide-field fluorescent microscopy image of the assembled clusters from an overlaid z-stack in Fig. 6c, it is obvious that the sticky ends at the tips of the flat DNA origami L-belt enabled the construction of colloidal clusters with precisely controlled binding angles, positions, dihedral angles, and chiralities.<sup>55</sup> According to their basic design, any desired patterns or clusters can be further formed by wrapping a colloid in networks of crosses and belts.

### 3. Regioselective encoding with DNA patches

#### 3.1 Shape dependent DNA patches

The effective attraction between DNA-grafted colloids is the basis of programmable self-assembly. Rogers and colleagues have examined how colloidal particles can be integrated with DNA to build materials across a wide range of length scales, from the molecular scale to nanometers and micrometers.<sup>25</sup> According to the understanding of how specific interparticle attractions arise from DNA hybridization, the transient formation of bridges pulls the particles together, while various repulsion forces, including compression of the grafted DNA molecules, steric repulsion, electrostatic repulsion, and others,

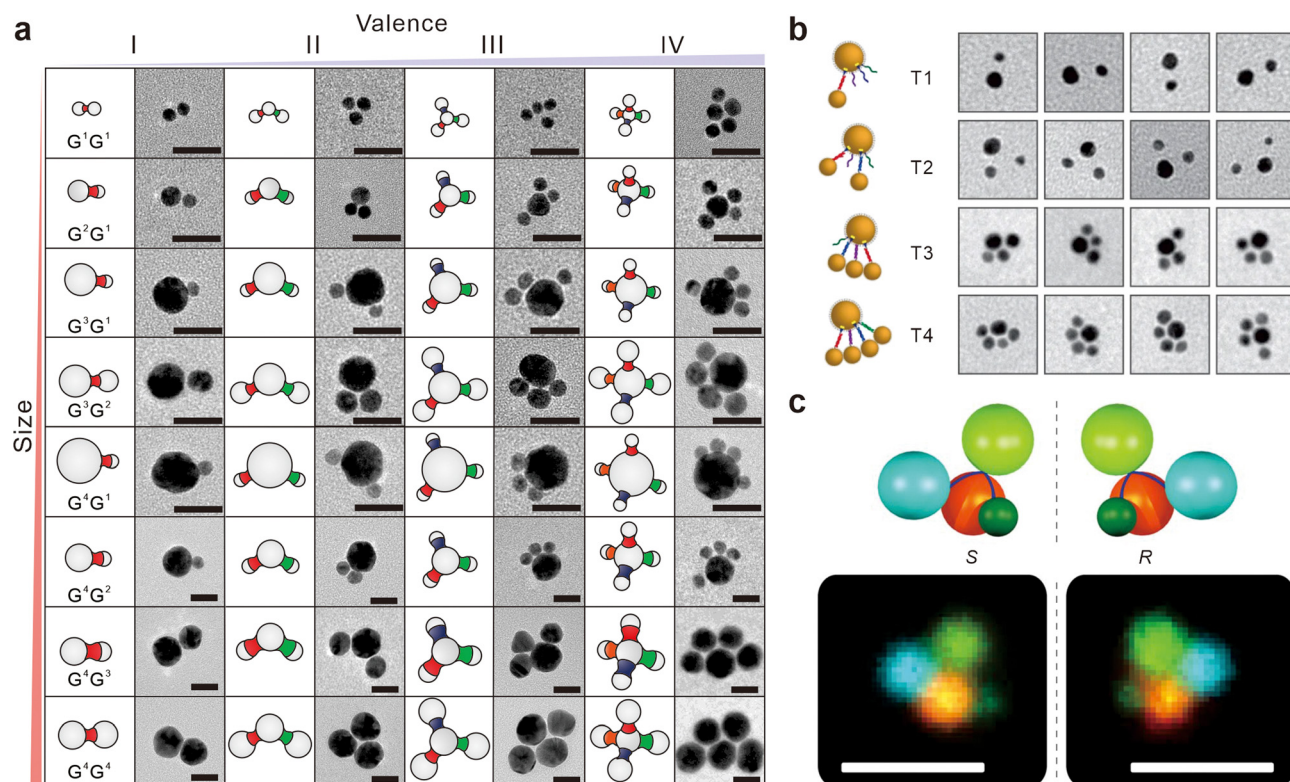


**Fig. 6** Assemblies constructed from colloids encoded with number-defined DNA molecules. (a) Schematic illustrations and transmission electron microscope (TEM) images of colloidal oligomers assembled from anisotropic single-DNA encoded AuNPs. The size and valence increase from top to bottom, and from left to right, respectively (scale bar = 20 nm).<sup>54</sup> Copyright 2020, Macmillan Publishers Ltd. (b) Satellite structures constructed using AuNPs with patterned DNA bonds.<sup>66</sup> Copyright 2016, Macmillan Publishers Ltd. (c) DNA origami L-belt functionalized colloidal clusters with controlled binding angles, positions, dihedral angles, and chirality (scale bar = 2  $\mu$ m).<sup>55</sup> Copyright 2017, Association for the Advancement of Science (AAAS).

push them apart. The density of grafted strands, which regulate the number of DNA bridges, is crucial for the formation of self-assembled structures. Although the strategy of number-defined DNA molecules presented above is appealing for achieving topologically finite architectures from the bottom up, the construction of well-defined materials is limited by the not-so-robust strength of a single-DNA duplex bond. Another promising route is to control the placement of multiple DNA strands on selective regions of the particle surface. The resultant DNA patches can form highly directional bonds through programmable, specific, and reversible patch-patch interaction, allowing the facile self-assembly of complex superstructures.

Patchy interactions can arise naturally from the anisotropy in the particle shape. Because of the multiple localized surfaces that differ in their chemical or physical properties, anisotropic particles present selective regions and offer the most feasible approach for regioselective DNA modification. Synthetic techniques have been developed to produce different anisotropic nanoparticles, such as AuNRs, AuNCs and gold nanostars (AuNSs). The native surfactant coating required for the synthesis of these particles is less dense at areas of high curvature, making alkylthiol-functionalized DNA ligands easier to replace. As a result, it has been possible to control the location of DNA patches on the anisotropic AuNPs. For AuNRs capped with a bilayer of cetyltrimethylammonium bromide (CTAB), CTAB is

preferentially bound along the (100) facets on the side of AuNRs, as opposed to (111) facets at the ends of the AuNRs. The ends of the AuNRs are more chemically reactive to thiolated DNA. Through a two-step modification process, Kotov and colleagues immobilized two distinct DNA strands on the end and side regions of AuNR (16 nm  $\times$  50 nm), respectively (Fig. 7a).<sup>74,75</sup> The relatively low ratio of DNA to AuNRs in the first step is critical to the formation of shape-based DNA patches.<sup>76</sup> Notably, Takarada and colleagues conducted additional statistical analysis to demonstrate the region-selectivity of this method.<sup>77</sup> By taking advantage of the uneven chemical reactivity of surfaces, the edges and the top-bottom surfaces of gold nanoprisms can be regioselectively modified with two different ssDNA sequences<sup>78</sup> or double-stranded DNA sequences.<sup>79</sup> This surfactant-based strategy has also been proven applicable to upconversion nanoparticles.<sup>80</sup>

Highly anisotropic AuNSs are structures with multiple branches and sharp tips. Based on the strong and concentrated near-field enhancement at localized surface plasmon resonance wavelengths, Odom and co-workers developed the light-directed functionalization of anisotropic AuNPs with different DNA sequences.<sup>81</sup> As shown in Fig. 7b, the Au-S chemical bonds at the tips of the AuNSs (with a diameter of  $\sim$  40 nm) would be selectively broken under exposure to fs-laser pulses, leaving spaces for more DNA strand conjugation.

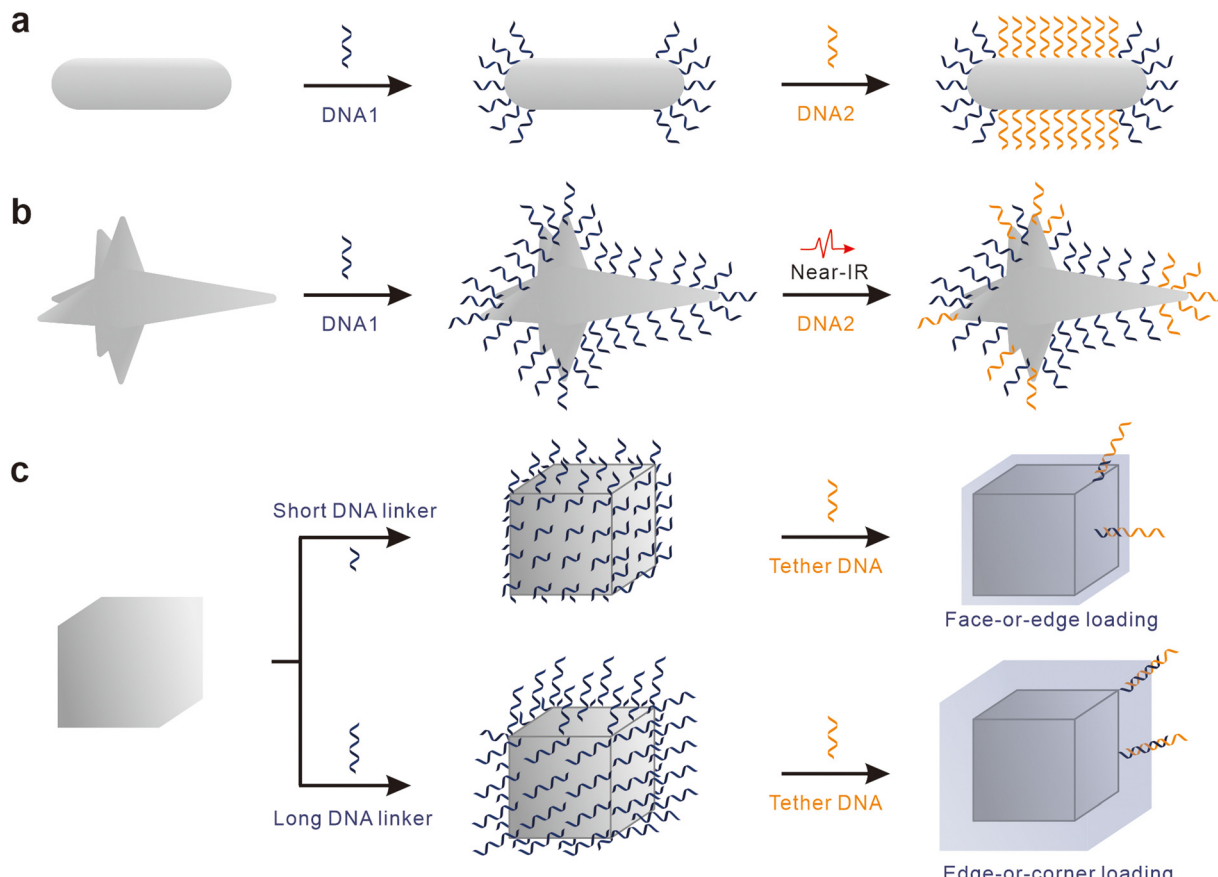


Fig. 7 Shape dependent DNA patches. (a) Regioselective modification of the AuNRs ( $16\text{ nm} \times 50\text{ nm}$ ) using two distinct DNA sequences.<sup>74</sup> (b) Schematic illustration of the light-mediated approach to regioselective modification of AuNSs (diameter:  $\sim 40\text{ nm}$ ).<sup>81</sup> (c) Length-dependent distribution of DNA linkers on anisotropic AuNCs (edge length:  $\sim 47\text{ nm}$ , corner curvature radius:  $\sim 8\text{ nm}$ ).<sup>82</sup>

Additionally, a recent study on anisotropic AuNCs with an average edge length of  $\sim 47\text{ nm}$  and corner curvature radius of  $\sim 8\text{ nm}$  has demonstrated that DNA strands of different lengths exhibited dramatically different behaviors when coating particles.<sup>82</sup> As shown in Fig. 7c, ssDNA was uniformly anchored to the surface of AuNCs, and subsequently duplexed with a complementary ssDNA linker containing a sticky-end overhang. The statistical analysis and theoretical predictions showed that the local linker grafting density highly depended on the chain length. In detail, short strands (16 nucleotides) preferred to graft on the cube's faces, while longer strands (86 nucleotides) preferentially bound to particle edges. For the nanoscale objects which exhibit a large variation in surface curvature, this length-dependent distribution of DNA linkers provides a facile and efficient method for the regioselective modulation of soft DNA shells.

### 3.2 Custom DNA patches

Compared to colloidal particles with anisotropic surfaces, the formation of DNA patches on isotropic colloids is more challenging. One conceptually straightforward way is to tune the particle surface accessibility prior to DNA modification.

A masking strategy has been proven effective to control the surface accessibilities and form Janus DNA patchy colloids. After trapping the isotropic particles on one substrate surface, such as planar substrates,<sup>83–86</sup> larger particles,<sup>87,88</sup> or emulsion,<sup>89</sup> only part of the particle surface would be exposed and available for subsequent DNA modification. For example, magnetic-bead supports with sizes of  $1\text{--}4\text{ }\mu\text{m}$  were used by Gang and colleagues to produce DNA-modified Janus AuNPs.<sup>87</sup> Because the hemisphere closest to the larger particle is electrostatically and sterically hindered, DNA strands can only hybridize with the hemisphere exposed to solution (Fig. 8a).

Similar toposelective surface modification strategies have been reported for the synthesis of DNA-grafted Janus AuNPs.<sup>88</sup> As shown in Fig. 8b, the bis(*p*-sulfonatophenyl) phenylphosphine (BSPP)-stabilized AuNPs were absorbed onto the surface of positively charged silica colloids due to the electrostatic interaction. Because of the strong interaction between gold and the mercapto group, BSPP stabilizers on the surface of AuNPs exposed to the solution were replaced by thiolated DNA, resulting in different geometric modifications. DNA-grafted Janus AuNPs were obtained by etching the silica beads with 10% HF (v/v) solution. In addition, the patchy diversity could be increased in combination with the molecular transfer method.

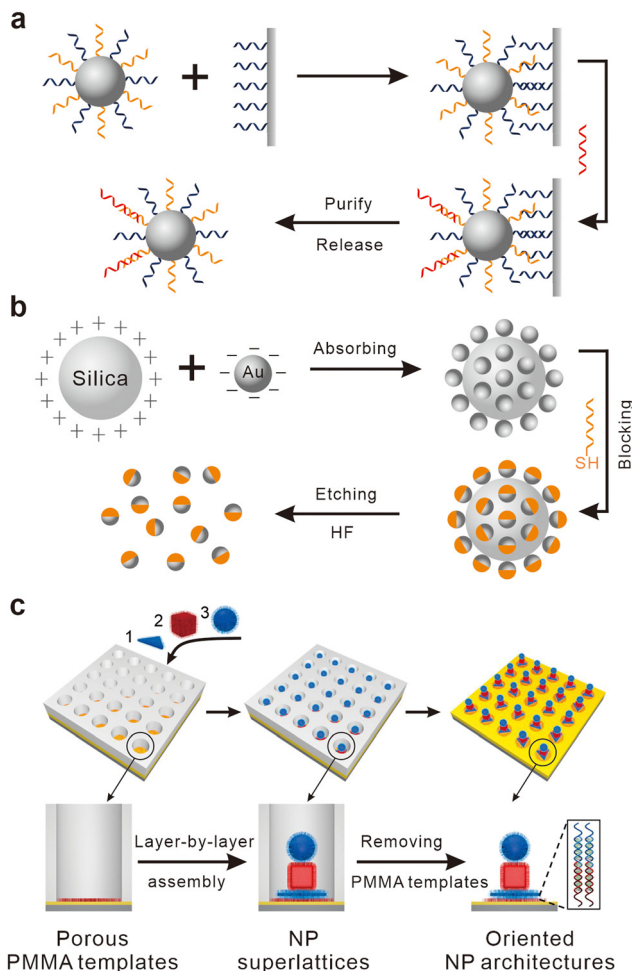


**Fig. 8** Physical masking strategies. (a) The encoding steps in fabricating DNA-modified Janus AuNPs on the surface of magnetic colloidal particles (1–4  $\mu\text{m}$ ).<sup>87</sup> (b) The toposelective surface modification strategy of DNA-grafted Janus AuNPs using silica particles as the masking support.<sup>88</sup> (c) Programmable assembly of DNA functionalized disk, cube and sphere gold nanoparticles in a confined 3D polymer template.<sup>90</sup> Copyright 2018, Association for the Advancement of Science (AAAS).

Micrometer-sized Janus particles with two distinct DNA patches were created by using a DNA-coated 2D gold surface as both the surface blocking support and the DNA transfer template. The area and density of DNA patches have been verified by fluorescent labeling.<sup>91</sup>

Moreover, a confined 3D hard template could be used to form predetermined site-selective DNA patches, enabling the template-assisted assembly of 2D nanoparticle arrays. By combining the advantages of regioselective masking with top-down lithography, large-area superlattices of discrete, reconfigurable nanoparticle architectures with DNA bonds were fabricated on a gold surface.<sup>90</sup> As demonstrated in Fig. 8c, an array of 1D pores was fabricated in a poly(methyl methacrylate)-coated gold substrate layer using top-down electron beam lithography. The gold surface at the bottom was densely modified with ssDNA containing a terminal propylthiol group, followed by hybridizing with the complementary oligonucleotides containing a

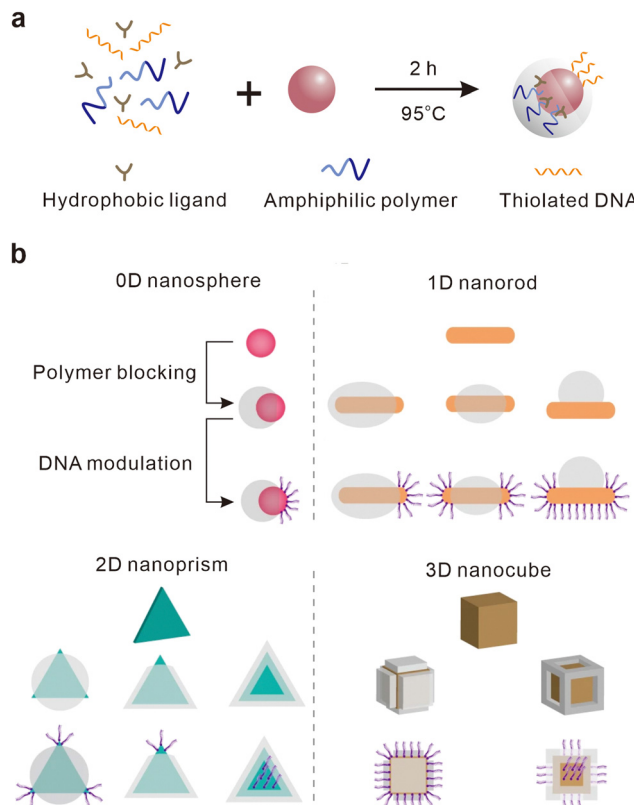


**Fig. 9** Chemical masking strategies. (a) DNA-grafted patchy nanoparticles prepared in one-pot synthesis using ligand competition.<sup>92</sup> (b) 0D, 1D, 2D and 3D regioselective surface encoding of nanoparticles through controllable polymer blocking and DNA modification.<sup>93</sup> Copyright 2019, Macmillan Publishers Ltd.

short “sticky end” overhang. As a result, the DNA functionalized disk, cube and sphere gold nanoparticles of controlled size could be immobilized in the pore though the Watson-Crick base pairing between complementary DNA sticky ends, forming DNA patches at the top surface of nanoparticles with the help of the 3D template. Consequently, predictable architectures of DNA-functionalized nanoparticles were assembled within each pore in a layer-by-layer manner by designing the sticky-end DNA sequence coated on the selected nanoparticles of special shapes to duplex with that of the layer below. After coating the superlattices with a thin layer of solvent with increasing ratios of ethanol to water, the average interparticle coupling distance would decrease, resulting in dramatic changes in their absorption spectra and corresponding surface color.

In addition to physically blocking the particle surface with substrates, colloidal DNA patches can also be fabricated by chemical blocking. Lu and colleagues demonstrated a one-step solution-based method to prepare patchy AuNPs (Fig. 9a).<sup>92</sup> In principle, this method is based on the competition between a hydrophilic ligand and a hydrophobic ligand on the AuNPs surface to induce anisotropic attachment. The attachment of hydrophobic polymer chains on the fully hydrophobic ligands covered AuNP surface during self-assembly resulted in a uniform outer layer. Introduction of an additional hydrophilic

ligand during the encapsulation caused an intriguing change in the polymer attachment, giving AuNPs with eccentric core/shell structures. When thiolated DNA molecules are used as the hydrophilic ligand, they serve as unique bulky ligands that allow efficient post-functionalization on the gold surface, enabling regioselective functionalization of DNA onto AuNPs and producing DNA patchy AuNPs. For the experimental details, the spherical AuNPs were incubated with a mixture of hydrophobic ligands (thiolated phospholipids, PSH), hydrophilic ligands (thiolated DNA strands) and amphiphilic polymers (polystyrene-*b*-poly(acrylic acid), PS-PAA) in dimethyl formamide (DMF)-H<sub>2</sub>O binary solvent. The ratio of PSH to DNA was tuned to balance the competition between the two ligands. After heating at 95 °C for two hours and cooling to room temperature, spatially controlled DNA-modified Janus AuNPs were formed with high yield and high DNA density.

This chemical masking strategy is also applicable to anisotropic colloids and provides more sophisticated DNA patches. Weizmann and colleagues have expanded on the previously demonstrated partially encapsulated nanoparticles and achieved polymer-free surface regions at the nanoscale by controlling the interfacial tension between nanoparticles, solvent, and copolymer (Fig. 9b).<sup>93</sup> In detail, the partially polymer blocking was conducted in one pot by mixing AuNPs, amphiphilic diblock copolymer (PS-PAA), hydrophobic ligands (PSH), and hydrophilic ligands (2-methylaminoethanol, 2-MAE) in a DMF-H<sub>2</sub>O solvent mixture. The polymer-blocked surface area of nanoparticles can be tuned by carefully tuning the interfacial free energies of this ternary system. After polymer blocking, the surface ligands (including hydrophobic and hydrophilic ligands) on the polymer-blocked surface area could be replaced with thiolated ssDNA, enabling regioselective DNA patches on the zero-dimensional (0D) nanosphere (with diameters of 20 and 30 nm), 1D nanorod (with the aspect ratio 3.9,  $L = 54.3 \pm 3.4$  nm,  $W = 14.1 \pm 1.1$  nm), 2D nanoprisms (with an edge

length of  $72.7 \pm 10.6$  nm), and 3D nanocube (with an edge length of  $44.4 \pm 2.6$  nm).

Regioselective modification of the colloid with directional DNA patches in three-dimensions remains a challenge.<sup>2</sup> To overcome this barrier, colloidal particles with a range of well-controlled 3D bonding symmetries have been investigated.<sup>13,41,94</sup> The milestone work is the fabrication of micrometre-sized colloidal particles with different numbers of patches (1–7 and higher) that adopt spherical, linear, triangular, tetrahedral, trigonal dipyramidal, octahedral, or pentagonal dipyramidal symmetries.<sup>17,95</sup> These DNA patchy bonds precisely mimic the multivalent bonding modes of atomic orbitals, including sp, sp<sup>2</sup>, sp<sup>3</sup>, sp<sup>3</sup>d, sp<sup>3</sup>d<sup>2</sup> and sp<sup>3</sup>d<sup>3</sup>. As shown in Fig. 10a, the synthetic approach started with clustering the amine-modified polystyrene spheres into polyhedron-like geometries. The clusters were then swollen and polymerized from the centre outwards to the extent. Only small patches remained from the original spheres, while the swollen interior portion was inert. The remaining amine-terminated domains could be further functionalized with DNA strands via the biotin-streptavidin linkage, resulting in multivalent DNA patches oriented in well-defined geometries. The valence, symmetry, and patch size could be well controlled by varying the degree of emulsification and swelling. In addition, other monofunctional,<sup>96</sup> bifunctional,<sup>97–99</sup> trifunctional<sup>100</sup> and tetrafunctional<sup>101</sup> DNA patchy colloids have also been developed in conceptually similar approaches.

One impressive alternative strategy is to use colloidal crystals as templates to generate faceted DNA patchy particles, where DNA is used to engineer the shape as well as to encode information on the colloidal particles (Fig. 10b).<sup>102</sup> In this work, two deformable emulsion droplets containing a photo initiator were coated with complementary DNA strands and formed binary crystals. Due to the mobility of DNA on the droplet surface, the DNA strands were recruited to and

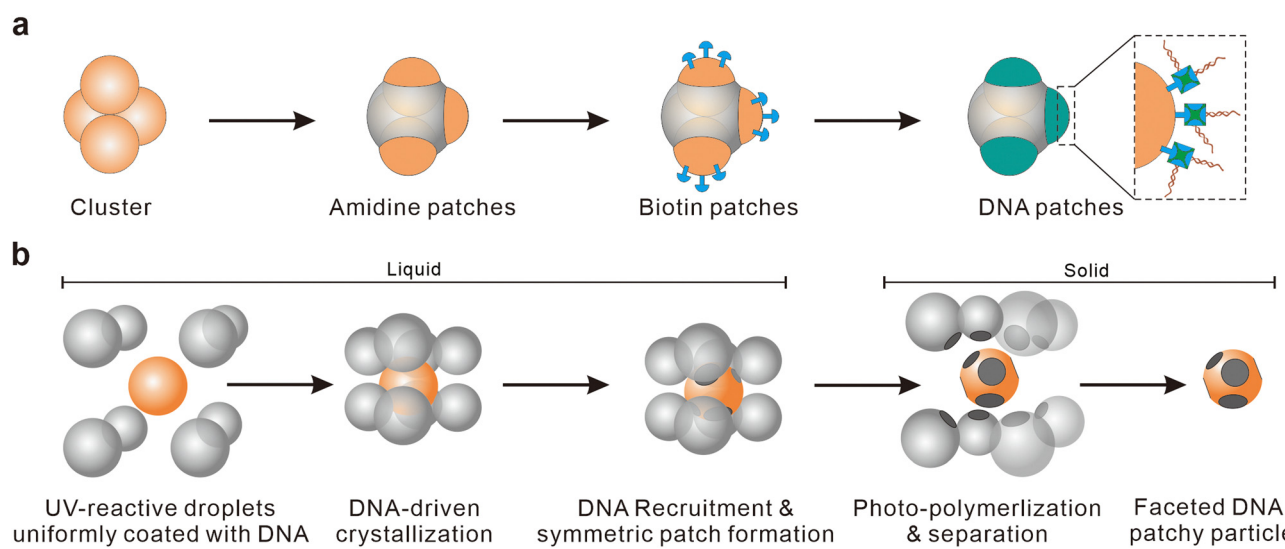


Fig. 10 Colloids with valence and specific directional bonding. (a) The swelling and functionalization method for creating the colloidal atoms with DNA patchy valence.<sup>17</sup> (b) Schematic of the production of faceted DNA patchy colloids using a photo-printing method.<sup>102</sup>

ultimately localized at droplet junctions, resulting in DNA-encoded faceted patches. Multivalent faceted patchy particles were finally produced after solidification of droplets by rapid photo-polymerization under UV light. Notably, the facet size and DNA distribution are determined by the balance between the DNA binding energy and the elastic deformation energy of droplets. When the temperature was raised above the melting temperature, the resulting solid particles dissociated, releasing individual faceted DNA modified particles for further use.

### 3.3 Programmable assembly of DNA patchy colloids

Simulations with patchy colloids revealed that patchy interactions are required to form a wide range of assemblies.<sup>38,103,104</sup> Regioselective DNA patches enable the formation of complex core-satellite clusters. As shown in Fig. 11a, anisotropic core-satellite clusters were created by selective incorporation of DNA patches at the end (i) or side (ii) of AuNRs (Fig. 7a),<sup>74</sup> at the tips of AuNSs (iii) (Fig. 7b),<sup>81</sup> or at the edges of gold nanotriangles (AuNTs) (iv).<sup>79</sup> Similarly, DNA patches decoration on isotropic particles enabled the specific assembly of either well-defined dimer nanoclusters or multivalent Janus nanoclusters.<sup>87</sup> Instead of using a single DNA patchy particle to hybridize with isotropic particles, all patchy particles (Fig. 9a) demonstrated better spatial control during self-assembly (Fig. 11b).<sup>92</sup> AuNCs with multivalent DNA patches on their six facets or edges have been created through controllable polymer blocking and regioselective DNA modification (Fig. 9b). The monovalent patchy AuNPs can be bound to the faces or vertices of multivalent patchy AuNCs separately (Fig. 11c).<sup>93</sup>

Micrometer-sized colloidal particles with DNA patches are appealing for colloidal self-assembly due to their potential photonic applications. The patchy bonds provide essential information that provide colloids with specific and directional interactions.<sup>17,41</sup> Depending on the Janus balance related to the mutually attractive fractional surface area of particles, DNA-grafted Janus colloids could self-assemble into diverse structures, including micelles, chains, vesicles, bilayers, and rings.<sup>96</sup> Reconfigurable and reversible transitions have been realized between the colloidal 1D chains and 2D bilayers using toehold strand displacement and external temperature stimulation.<sup>99</sup> Furthermore, the synergistic effect of patchy DNA bonds and entropic depletion interactions was used to program colloidal superstructures. As shown in Fig. 11d, the triblock Janus colloids could be assembled into 2D or quasi-2D superstructures by controlling the patch sizes and tuning the temperature conditions.<sup>97</sup> For the triblock Janus colloids with  $\theta = 86^\circ$  ( $\theta$  is defined as half of the opening angle), flower-like Kagome structures were formed when annealing at 41–46 °C and brick wall-like structures were formed when annealing at 57–62 °C. In particular, annealing at 47–53 °C leads to the coexistence of the two structures.

As demonstrated, DNA patchy particles display distinct, directional self-assembly behavior, allowing complex structures to be programmed based on the size, amount, and arrangement of the patches.<sup>30</sup> Their potential in higher-order assembly has also been investigated. Pine, Sacanna, and colleagues

fabricated the tetrahedral-shaped particles with four retracted DNA patches by selectively functionalizing the central domain of colloidal tetramers.<sup>101</sup> The center DNA patches were carefully designed to retract their radial extent from the plane produced by the spherical lobes. By combining the directional DNA interactions with a steric interlock mechanism, the lobes on different tetramers were orientated in the correct staggered conformation while avoiding other isomers. The function of the particle lobes is to alter the orientation during colloidal nucleation. When this unique arrangement occurs on a larger scale, it produces perfect cubic diamond colloidal crystals (Fig. 11e).

## 4. Regioselective encoding with DNA origami shells

### 4.1 Encoding colloids with DNA origami shells

Despite the fact that DNA patchy particles enable specific and directional interactions, orthogonal DNA interaction is another rapidly rising direction in regioselective surface encoding. Chromatic patchy colloids with orthogonal interactions have been demonstrated to self-assemble into the desired superlattice by Brownian dynamics simulations.<sup>38</sup> Conceptually, the bonding properties of the guest particle can be determined by the host shell when isotropic particles are encapsulated inside a tailored shell. This design strategy provides another way to give particles pre-designed bonding properties. DNA molecules can form various geometries and motifs beyond the standard double helix. After enhancing the rigidity of DNA structures by packing multiple DNA helices *via* a series of immobile Holliday junctions,<sup>105,106</sup> a wide range of DNA structures has been created using DNA structural nanotechnology, most notably through DNA origami.<sup>21,107</sup> DNA origami has been identified as the appropriate host shell for colloidal self-assembly, allowing for control over the binding orthogonality.

In 2011, Yan and co-workers achieved spatial orientation control of nanoparticles using addressable DNA origami nanocages to encapsulate AuNPs.<sup>108</sup> The origami capsule disrupted the symmetry of spherical nanoparticles and offered a platform for further functionalization. Gang and colleagues developed a square-shaped DNA frame that encased an isotropic particle (gold, 10 nm diameter). The DNA interaction was defined as a “colored” valence of four with a planar, square binding coordination (Fig. 12a).<sup>42</sup> Sleiman and colleagues introduced 3D orthogonal bonding to AuNPs by embedding them with wire-frame DNA structures.<sup>109</sup> Moreover, a variety of polyhedral-shaped DNA framework nanocages formed by DNA motifs have been developed to swallow the AuNPs,<sup>110,111</sup> providing the spherical particles with well-defined valences, orthogonality, and bonding directions.<sup>111</sup> The spherical nanoparticle core can be replaced by other particles for encapsulation. For instance, an open DNA origami clamp, consisting of two half-tubes linked by two flexible hinges, was designed for AuNR encapsulation.<sup>112</sup> Taking advantage of DNA origami’s flexibility, a one-pot method has been developed to prepare multivalent nanoparticles with DNA origami directed patches. The

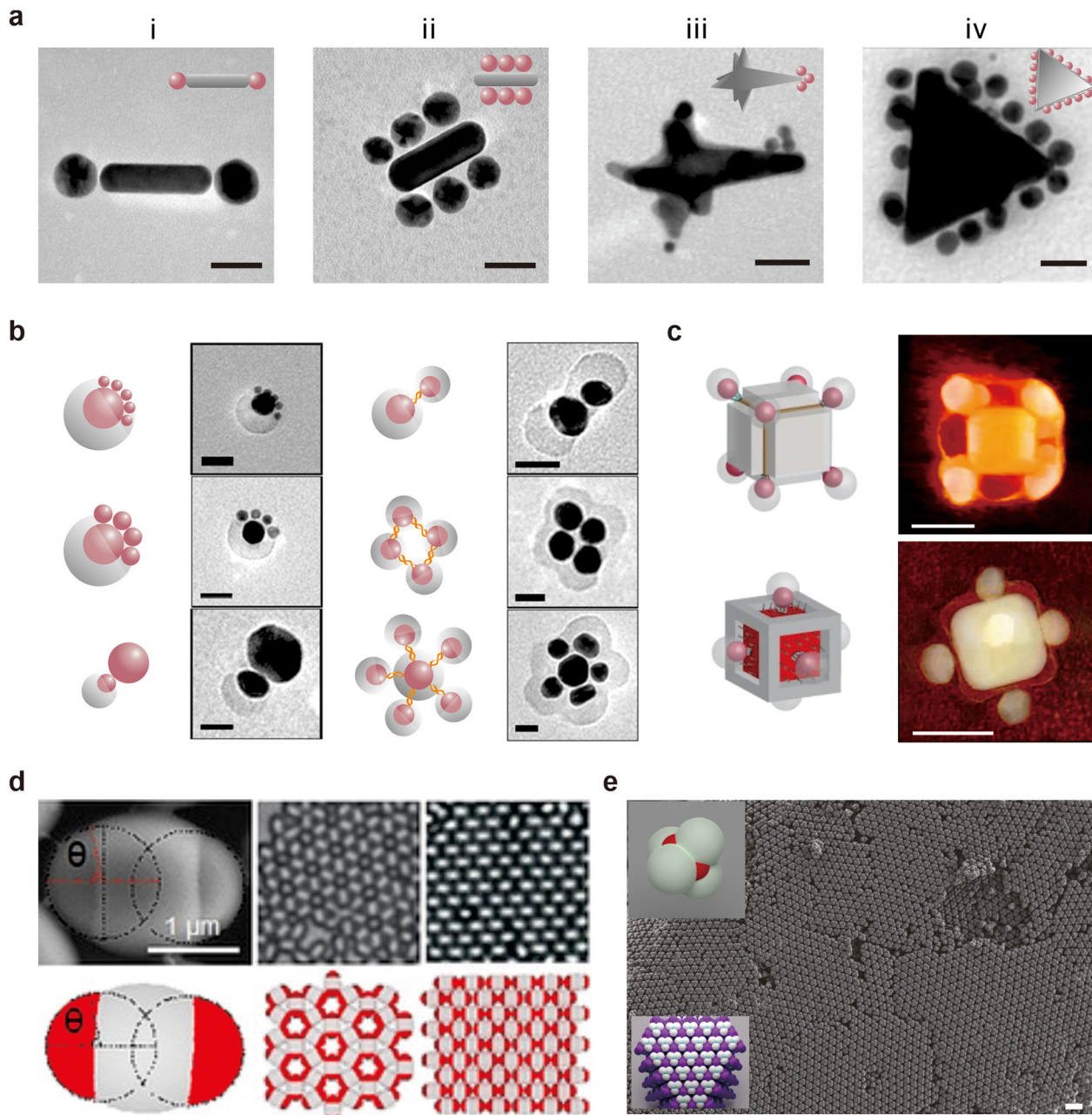


**Fig. 11** Assemblies constructed from DNA patchy colloids. (a) Core-satellite clusters constructed by regioselective DNA encoded anisotropic nanorods (i and ii),<sup>74</sup> nanostars (iii),<sup>81</sup> and nanoprisms (iv)<sup>79</sup> with isotropic SNAs (scale bar = 25 nm). (i and ii) Copyright 2012, American Chemical Society. (iii) Copyright 2021, American Chemical Society. (iv) Copyright 2019, Multidisciplinary Digital Publishing Institute. (b) Cluster structures built by combining Janus patchy AuNPs with isotropic nanoparticles (left) or Janus patchy AuNPs with Janus patchy AuNPs (right) (scale bar = 25 nm).<sup>92</sup> Copyright 2013, American Chemical Society. (c) Tomogram reconstructions of the assemblies of Janus AuNPs bound to the vertices (up) or faces (down) of AuNCs (scale bar = 50 nm). Images reproduced with permission.<sup>93</sup> (d) Colloidal superstructures assembled by triblock Janus particles with  $\theta = 86^\circ$ .<sup>97</sup> From left to right: Scanning electron microscope (SEM) image (top) and schematic illustration (down) of triblock Janus particles, flower-like Kagome structures and brick wall-like structures. Copyright 2021, Wiley-VCH Verlag GmbH & Co. (e) Colloidal cubic diamond via DNA-mediated assembly of the tetrahedral patchy particles (scale bar = 5  $\mu\text{m}$ ).<sup>101</sup> Copyright 2020, Macmillan Publishers Ltd.

DNA-coated AuNPs (with a diameter of 15 nm) were annealed with the DNA scaffold and staple strands together. The valence and dihedral angle of the interactive patches could be well controlled by the design and co-assembly of particle nano-flowers (Fig. 12b).<sup>113</sup>

This encapsulation strategy can be further developed with 3D structural DNA origami frameworks, where both internal binding and external DNA interaction patches can be rationally designed.<sup>115</sup> As illustrated in Fig. 12c, Gang and colleagues reported the *de novo* design of DNA-prescribed and valence-

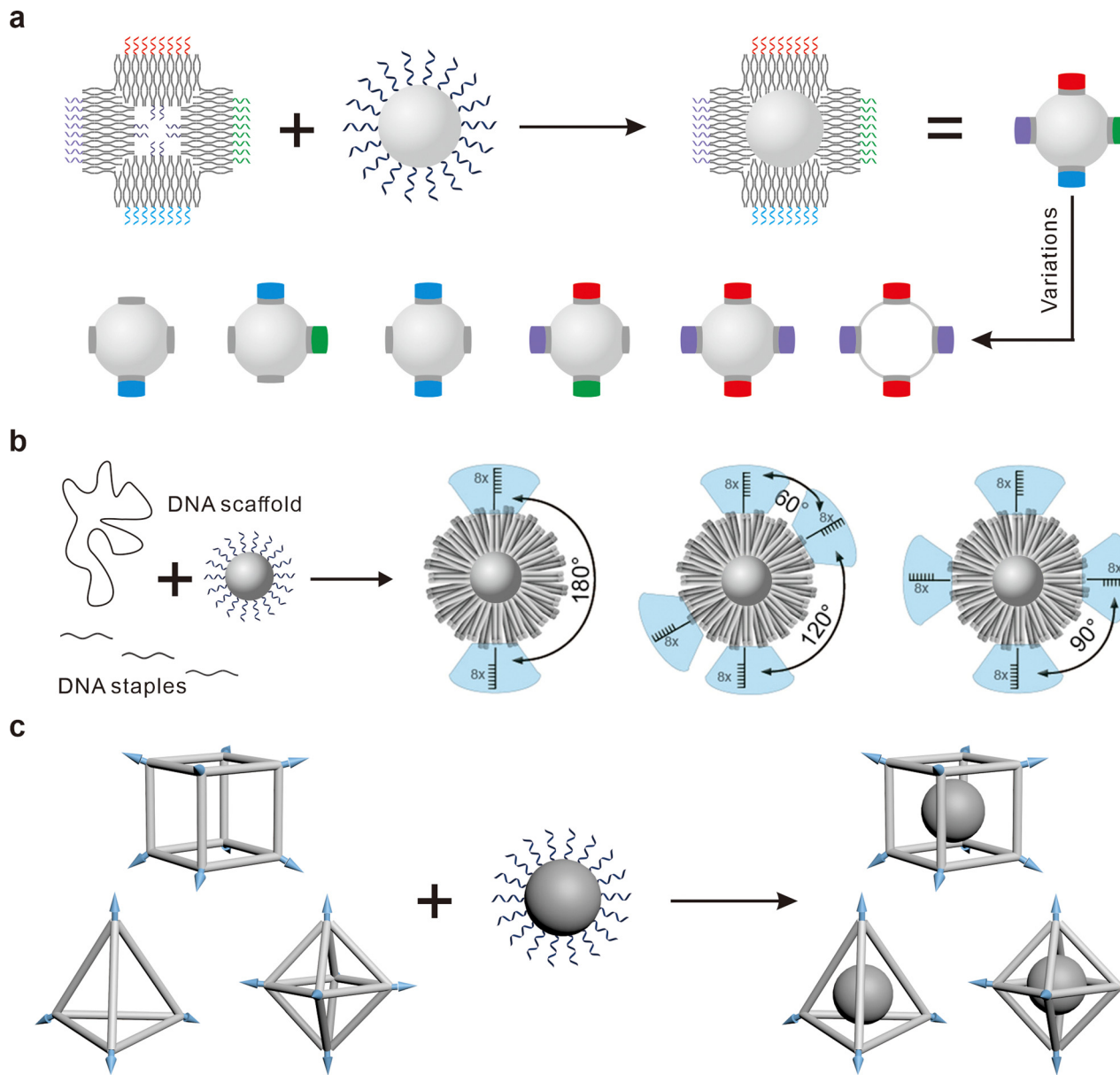


**Fig. 12** Regioselective encoding of colloids with DNA origami shells. (a) Orthogonal DNA bond interactions provided by the introduction of a square-like DNA frame surrounding isotropic AuNPs (10 nm).<sup>42</sup> (b) Schematic illustration of the one-pot fabrication process of multivalent colloidal AuNPs (15 nm) with DNA nanoflower directed patches.<sup>113</sup> Adapted and modified with permission from ref. 113. Copyright 2016, American Chemical Society. (c) The formation of 3D DNA origami framework-prescribed and valence-controlled material voxels.<sup>114</sup>

controlled “material voxels” using polyhedral DNA origami frameworks.<sup>114,116</sup> The interior origami volume could be used to incorporate various nanomaterials ranging from inorganic (AuNPs and QDs) to bio-organic (proteins), while the outside framework constructed a patchy shell around the nanoparticles. Very recently, AuNPs in specific cluster arrangements have been encapsulated in DNA tetrahedral frames to program the clusters’ valence.<sup>117</sup> Using 3D hexagonal prism DNA origami as a building block, Wang and colleagues demonstrated the feasibility of building finite hierarchical nanoarchitectures with complicated conformations through orthogonal and directional DNA bonding.<sup>118</sup> The DNA bonds of the origami enclosed

particle could be defined in 3D space by the external origami toolboxes, which offered great opportunities for fabricating complex functional nanoarchitectures.<sup>117–122</sup> Moreover, the surface chemistry and nanoscale positioning of QDs can also be spatially addressed using wireframe DNA origami.<sup>58</sup>

#### 4.2 Programmable assembly of colloids encoded with DNA origami shells

Following the host-guest interaction between nanoparticles and DNA nanostructures, the resultant DNA origami enclosed colloids would have nanoscale addressability inherent in the DNA origami shells. As shown in Fig. 13a, the surface of AuNRs

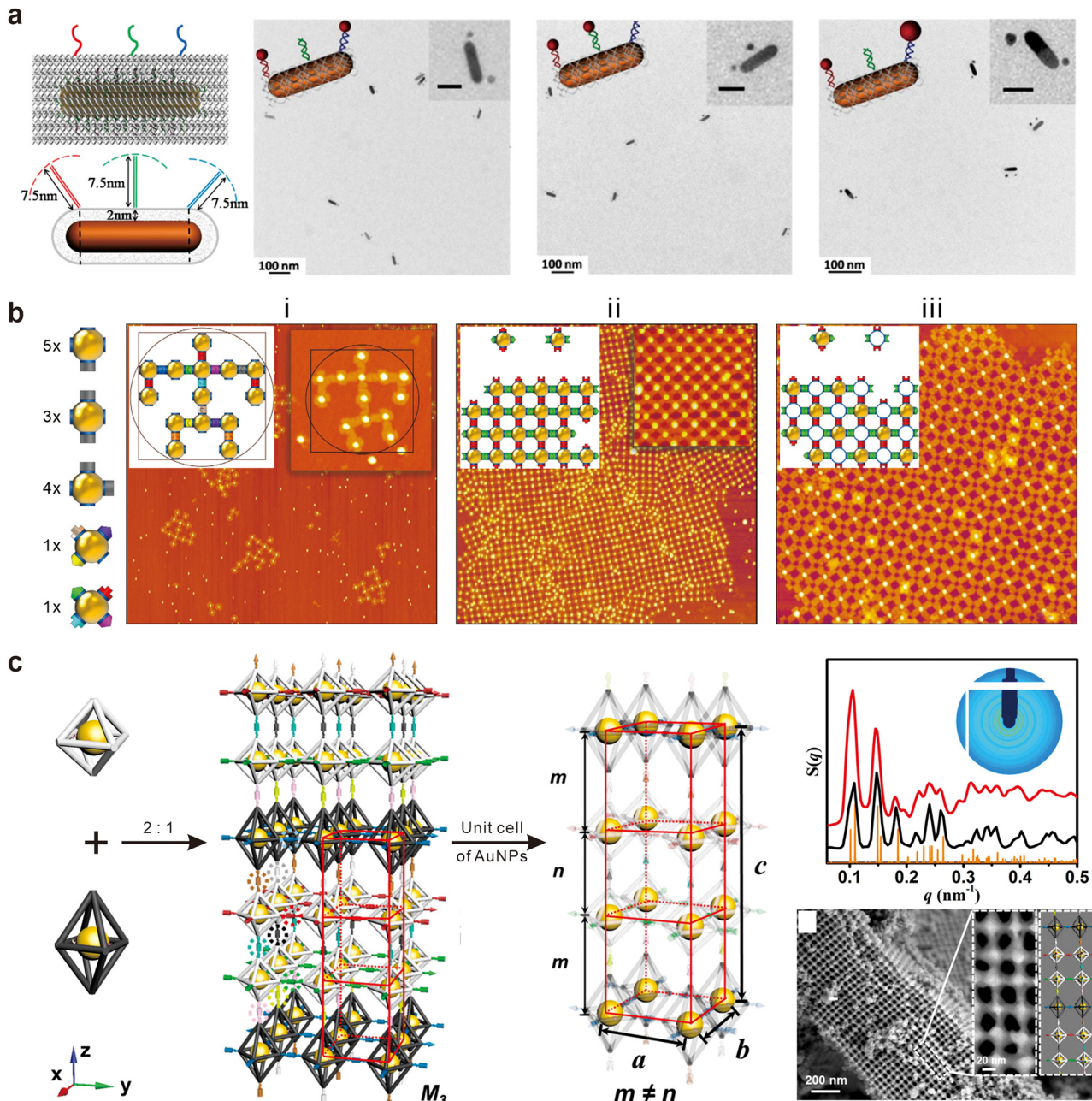


**Fig. 13** Assemblies constructed from colloids with DNA origami shells. (a) Schematic illustration of DNA origami clamp encapsulated AuNRs ( $13\text{ nm} \times 38\text{ nm}$ ) and TEM images of AuNR and AuNP assemblies.<sup>112</sup> Copyright 2016, American Chemical Society. (b) Schematic illustration and atomic force microscope (AFM) images of the non-periodic (i) and periodic (ii and iii) structures from orthogonal particles encapsulated by the 2D DNA origami frames (Scale bar = 200 nm).<sup>42</sup> Copyright 2016, Macmillan Publishers Ltd. (c) Schematic illustration of co-crystallization of regular octahedral and elongated octahedral particles. The corresponding small-angle X-ray scattering (SAXS) patterns and representative low voltage high resolution SEM images are shown on the right.<sup>119</sup> Copyright 2020, American Chemical Society.

has been precisely tailored by the sequence and position of the DNA bonds protruding from the DNA clamp shell, including the chemical valence from monovalent to divalent and trivalent, as well as site-specific modification from the top to the middle and bottom of the AuNR. As a result, different patterns of AuNP-AuNR heterostructures were constructed in high yield.<sup>112</sup> In another strategy, DNA tetrahedra encapsulated nanoparticles could only hybridize to complementary particles

via the four faces of the nanoarchitecture, resulting in molecular-like cluster assemblies.<sup>111</sup>

Aside from defining the direction of bonding interactions via DNA origami shells to organize patchy particles, orthogonal bonding can also be used to organize various topological types of nanoparticle assemblies. For example, the chromatic platform developed by the Gang Group (Fig. 12a) allowed the prescribed assembly of both non-periodic and periodic

Published on 31 July 2023. Downloaded by East China University of Science & Technology on 10/9/2023 3:46:17 AM.

structures arising from different origami-encapsulated particle subsets (Fig. 13b).<sup>42</sup> As shown in the AFM images, an anthropomorphically shaped nanocluster (i) was created by mixing fourteen particles within five topological classes of modules at specific stoichiometries. Two 2D square arrays (ii and iii) might appear to be two equivalent forms, but in fact, they are structurally identical lattices with differing object-binding specificities. Moreover, they were constructed with high spatial integrity and exceptional micrometer domain sizes. In contrast to these square lattices obtained with four valence sites at 90°, hexagonal lattices could be achieved by separating the four binding sites at approximately 120° and 60°.<sup>113</sup> In particular, the assembly of the orthogonal patchy particle model has also been theoretically studied in 3D space.<sup>38</sup> It is thought that orthogonal bonds in 3D spaces would enable the generation of structures that would not be possible with a single bond type. For example, orthogonal and directional interactions have been built by minimizing the thorny non-specific interactions between hexagonal prismatic DNA origami. Unlike many infinite periodical structures, a library of finite superstructures with well controlled 3D conformations was readily constructed through this orthogonal platform.<sup>118</sup>

The DNA origami octahedron is a representative frame shell to predefine the patch valence with a controlled number, direction, and orthogonality (Fig. 12c). In addition to the 1D and 2D architectures assembled by the node-and-spacer approach,<sup>122</sup> these DNA octahedra encoded particles could be assembled *via* a specified co-crystallization approach.<sup>114,119,121</sup> As evidenced by SAXS and high-resolution SEM imaging in Fig. 13c, a complicated lattice (the parameters of the unit cell are as follows:  $a = b = 58$  nm,  $c = 191$  nm,  $m = 66.5$  nm,  $n = 58$  nm) has been successfully synthesized by mixing two different building blocks with a ratio of 2 : 1 *via* a sophisticated packing mode.<sup>119</sup> The produced lattice M3 could be considered as the repeating combination of one layer of elongated octahedral particles and two layers of regular octahedral particles. In particular, nine distinct orthogonal bonds protruding from the DNA origami shells are required for the high complexity of the lattice. More types of particles with orthogonal and directional patches are expected to expand the library of dynamic 3D superstructures and lattices.<sup>123,124</sup> Recently, 85 types of DNA origami frame/AuNPs superlattices have been obtained using three different DNA origami platforms (the regular octahedron, the elongated octahedron, and the partially elongated octahedron) as building blocks.<sup>125</sup>

## 5. Collective properties and emerging applications

The development of regioselective encoding enables the DNA molecules to be placed in discrete locations on individual colloids. The formed anisotropically modified colloids show novel properties that are different from those of isotropically functionalized colloids. One elegant example is the single DNA-wrapped QDs produced by steric exclusion. These monovalent

QDs can not only retain their small size and excellent photophysical properties, but also incorporate a single, modular targeting functionality. As a result, they have been utilized as modular and nonperturbing imaging probes to track individual notch receptors on live cells.<sup>50</sup> Similarly, monovalent QDs have been employed as imaging tags to visualize the microtubules in HeLa cells.<sup>53</sup> Another typical example is the DNA-grafted Janus AuNPs. Half of the surface modified with thiolated DNA molecules is catalytically active, while the other half remains inactive due to the dense BSPP. Due to their catalytic and nanoplasmonic properties, they exhibited self-thermophoresis behavior.<sup>88</sup> In addition, the surface modification of gold nanoclusters with a single ssDNA molecule could transfer ~90% hydrophobic clusters into an aqueous solution. There was a 13-fold increase in the fluorescence quantum yield of gold nanoclusters, and the surface-constrained DNA molecule retained the specific recognition ability for biosensing.<sup>59</sup>

This DNA-based asymmetry enables the formation of various regiospecific assemblies, whose collective properties are controlled not only by colloidal properties but also by the symmetry, orientation, and size of the assembled structures. Chirality is a key feature of the biologically-essential molecules and materials. When DNA-directed regiospecificity meets non-covalent assembly of artificial chiral structures, it brings supramolecular chirality that is not possessed by isotropic superlattices made from uniformly DNA-grafted colloids. For example, the anisotropic ‘four-particle’ colloidal molecules fabricated with SSE-encoded PANs exhibited an intense negative peak at the plasmonic absorption region (~530 nm) in the circular dichroism spectrum (Fig. 14). Theoretical calculations further confirmed their asymmetric distribution of electric current density under left- or right-handed circularly polarized light at 530 nm.<sup>54</sup> Since chirality is a key feature of chemical and biological molecules, these assembled colloidal structures with plasmonic chirality showed potential in photonic biosensing.<sup>74</sup> Chiral assemblies constructed by regiospecific AuNRs have promising attomole detection limits in DNA detection. The limit of detection for target DNA markers is as low as 3.7 aM, which is greatly needed for medical diagnostics, forensics and environmental needs.<sup>75</sup>

The utilization of DNA nanotechnology in plasmonics and photonics has led to novel research directions. Introducing the nanoparticles with DNA-based anisotropic surface chemistry paves the way for designing spatially directed organizations, where the structural information is pre-encoded in the regiospecific surfaces of the components that make up the system. For example, the regiospecific plasmonic nanoscale superstructures (Satellite, Side and End isomers) composed of regiospecific AuNRs and SNAs presented different spectral behaviours that depending on the coupling mode of Raman scattering are significantly amplified in the gaps of plasmons.<sup>74</sup> Due to the excitation of localized surface plasmons, plasmonic nanostructures, give rise to surface enhanced Raman spectroscopy (SERS). The SERS intensity for regiospecific plasmonic assemblies was found to depend mainly on the number of particles in the assemblies. The degree of structural control made it

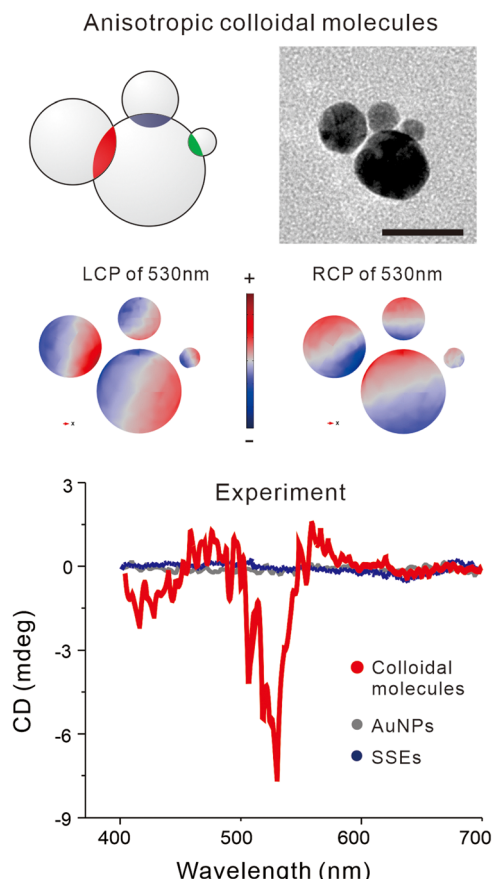


**Fig. 14** Single-stranded DNA encoded colloidal molecule with anisotropy and chirality. The anisotropic colloidal molecule was assembled by the 20 nm trivalent PANs with monovalent PANs of different sizes (5 nm, 10 nm and 15 nm) (Scale bar = 20 nm). The simulated distribution of their electric current density at 530 nm of left- or right-handed circularly polarized light was performed using the commercial software COMSOL Multiphysics based on a finite element method.<sup>54</sup> Adapted and modified with permission from ref. 54 and authors. Copyright 2020, Macmillan Publishers Ltd.

possible for these assemblies to probe the local organelle environment in live cells. Besides the particle numbers, positioning of metal particles within individual assemblies also plays a key role to the amplification of SERS signals.<sup>69,72</sup> DNA origami-mediated regioselective encoding makes it available to accurately control the positions of nanoparticles. As shown in Fig. 15, the plasmon coupling between the sharp curvature of the AuNCs (vertices and edges) and round AuNP surfaces would generate higher SERS signals than that between the flat faces of AuNCs and round AuNP surfaces.<sup>69</sup>

For the 2D superlattices built from individual colloidal plasmonic structures with different shapes, DNA bonds can be further designed to be dynamic.<sup>90</sup> The interparticle distances can contract and expand reversibly with a solvent polarity response, allowing the reconfigurable optical properties. The ability of regioselective assembly to control the spacing, sequence and arrangement of nanoparticles within each architecture is critical to the realization of tunable broadband absorption.

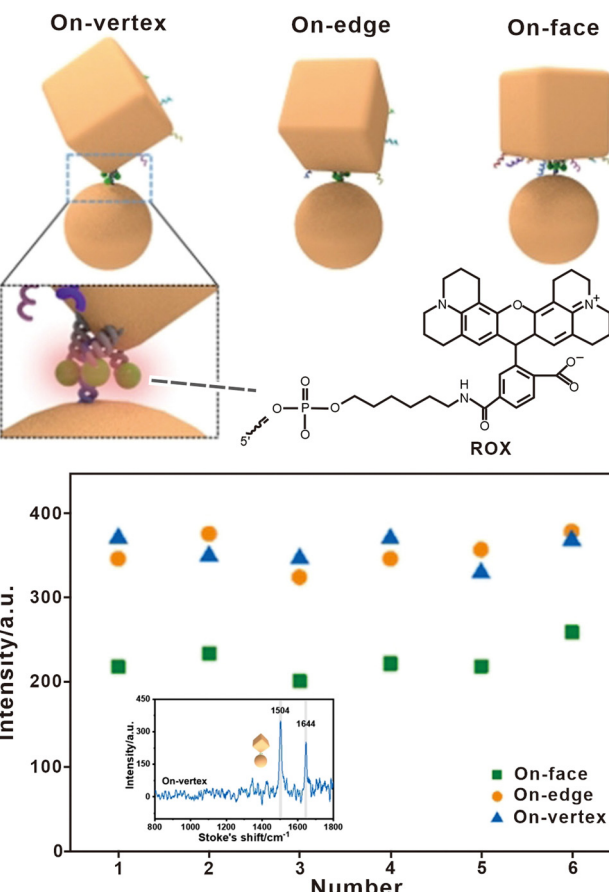


**Fig. 15** Single-molecule SERS measurements of three types of AuNC-AuNP plasmonic nanostructures containing three carboxy-X-rhodamine (ROX) Raman probes.<sup>69</sup> Adapted and modified with permission from ref. 69. Copyright 2021, Wiley-VCH Verlag GmbH & Co.

In three dimensions, the regioselectively functionalized colloidal particles have been applied in the construction of photonic crystals and photonic devices. A colloidal cubic diamond has been self-assembled by using partially compressed tetrahedral clusters with retracted sticky patches.<sup>101</sup> The colloidal particles in this diamond structure are directly connected, highly constrained, and mechanically stable, in contrast to the diamond superlattice produced by tetrahedral DNA origami with AuNPs.<sup>115</sup> The diamond structure, in particular, is well preserved after drying the suspension. The widest photonic bandgap of the obtained diamond structure is achieved at a compression ratio of 0.6. However, the cubic diamond colloidal crystals were assembled from polystyrene and 3-trimethoxysilylpropyl methacrylate, whose refractive indices of 1.6 and 1.4, respectively, are too low to open the photonic band gap. Therefore, using the colloidal systems as templates to make the inverse diamond structure with high-refractive-index materials such as TiO<sub>2</sub> will be promising in making optical devices. The obtained colloidal diamond has a lateral dimension of 80 μm and a thickness of 40 μm. Strategies leading to crystals with a larger lateral extent should be used to fabricate optical waveguides, lasers, and other optical applications.

## 6. Summary and outlook

Although the concept of DNA-mediated anisotropic functionalization of particle surfaces was first proposed in the mid-1990s,<sup>22</sup> a breakthrough in this field has occurred in recent years, especially with the boom in DNA nanotechnology. In this review, we have summarized the typical experimental strategies of imparting anisotropy to colloids with DNA for colloidal assembly, which fall into three categories: number-defined DNA molecules (Fig. 2a), DNA patches (Fig. 2b), and DNA origami shells (Fig. 2c). The DNA-grafted anisotropic colloids have been programmed to form 0D clusters, 1D chains, 2D arrays, and 3D lattices, which are difficult to achieve with isotropic DNA-coated colloids.<sup>54,99</sup> These bottom-up approaches provide unprecedented opportunities to create asymmetric assemblies from symmetric starting materials, which is particularly remarkable in materials science. Despite significant accomplishments, there are still numerous challenges.

First, each of the existing methods is only suitable for a narrow size range of colloids. For example, single-stranded DNA encoders are only appropriate for particles smaller than 30 nm. The DNA patches are difficult to create at the nanoscale size with the same accuracy as at the microscale. Despite DNA origami structures performing well to control matter at length scales less than 100 nm, larger DNA origami structures with micrometer size and precise nanoscale spatial addressability<sup>126,127</sup> are expected to naturally match up to larger colloids.<sup>55</sup> On the one hand, future work might focus on developing a versatile method to cover multiple sizes, ranging from several nanometers to several micrometers. On the other hand, control over the copy number and nanoscale positioning of atomically precise metal clusters (<3 nm) is critical to their application. It is also expected to see more attempts on exploiting the power of DNA-mediated regioselective surface encoding on noble metal nanoclusters. The chimeric ssDNA molecules and wireframe DNA origamis would be ideally suited to control their surface chemistry and properties.<sup>58,59,128</sup>

Second, the role of regioselective DNA bonds in colloidal self-assembly has not been thoroughly investigated. Although low-coordination colloidal molecules have been successfully constructed with particles at the nanoscale<sup>54</sup> and at the microscale,<sup>17</sup> there is still room to increase the complexity of non-periodic colloidal superstructures. Almost all patchy colloids have the same DNA patches on their surface, which severely limits the formation of non-periodic structures. Most regioselective surface encoding systems only exploit a limited number of DNA bonds (usually fewer than 3), while polychromatic and orthogonal DNA patches are engaged in the colloidal system to build intricate structures. By combining colloids with valence-programmable DNA origami shells,<sup>129</sup> it is expected that more nonperiodic mesoscopic structures, such as quasi-crystalline structures, can be created. In addition, the development of dynamic colloidal structures is just the beginning, and here DNA-mediated regioselective encoding technology opens

ample opportunities for switchable systems that depend on the distinct elements of regioselectivity, especially for the dynamic photonic and plasmonic systems. Moreover, the combination of this anisotropic bottom-up assembly with top-down nanofabrication technologies<sup>90</sup> is expected to enable the synthesis of even more sophisticated colloid-based architectures and multi-functional materials.

Third, the development of DNA-mediated regioselective encoding strategies towards self-assembly is impeded by challenges in revealing the complex nanoscale architectures at single particle level. In general, SEM or fluorescence microscopy is used to characterize micron-sized colloidal particles and their DNA-mediated assemblies. For the characterization of nanoparticles and their clusters, TEM, AFM, or cryo-electron microscopy can be employed, offering high resolution. When it comes to large-scale 3D superlattices formed by the assembly of nanoparticles, obtaining the complete structural information becomes challenging. To obtain a comprehensive structural understanding of these highly ordered superlattices, *in situ* characterization methods such as SAXS, liquid-phase TEM and optical microscopy are often combined with *ex situ* characterization techniques such as electron microscopy and ultramicrotomy. More significantly, a hard X-ray nanoprobe tomography has been developed recently to reveal 3D organization of a nanoparticle lattice with a size of 2 micrometers.<sup>130</sup> The positions of about 10 000 individual nanoparticles have been determined with 7 nm resolution. The tomographic reconstruction achieved at a single-particle level not only enables the inspection and volumetric analysis of occurring defects in superlattices but also clarifies the relationship between assembly motifs and lattices. In an effort to understand the structure of 3D superstructures at the single-component level and with elemental sensitivity, there is an anticipation that more powerful and convenient characterization methods will emerge.

Fourth, future research in the field of DNA-mediated regioselective colloidal assembly should focus on solving application-oriented requirements. Despite the creation of various colloidal clusters and superlattices, the particles in assembled architectures are not in close proximity to allow for efficient coupling due to the presence of DNA scaffolds.<sup>101,115</sup> One solution is to develop methods for reducing the interparticle distance while preserving the morphological shapes.<sup>90,111</sup> Since DNA itself does not have remarkable electrical, optical, or magnetic properties, another solution is to incorporate other functional components with DNA for specific applications. DNA metallization,<sup>131–133</sup> DNA silicification,<sup>134,135</sup> and DNA-based nanofabrication of conducting polymer<sup>136</sup> have demonstrated the possibility of producing functional DNA-colloidal materials. The method of solidifying DNA with silica<sup>137,138</sup> enables stabilizing the bulking materials made from anisotropic colloids and separating them from solutions into a state suitable for end use.<sup>121,139,140</sup>

All of this suggests that the field is poised for further development. Continued efforts toward DNA-mediated regioselective surface encoding will lead to new classes of assembled

architectures that unlock unique properties toward advances in optics,<sup>90,101</sup> photonics,<sup>101</sup> plasmonics,<sup>69</sup> catalysis,<sup>88,128</sup> bioimaging,<sup>50,53,74,80</sup> sensing,<sup>75,85</sup> and others.

## Abbreviations

0D	Zero-dimensional
1D	One-dimensional
2D	Two-dimensional
3D	Three-dimensional
AFM	Atomic force microscope
AuNPs	Gold nanoparticles
AuNRs	Gold nanorods
AuNCs	Gold nanocubes
AuNTs	Gold nanotriangles
AuNSs	Gold nanostars
BSPP	bis( <i>p</i> -sulfonatophenyl) phenylphosphine
CTAB	Cetyltrimethylammonium bromide
DNA	Deoxyribonucleic acid
ONP	Organic nanoparticle
PAEs	Programmable atom equivalents
PANs	Programmable atom-like nanoparticles
polyA	Polyadenine
PMMA	Polymethyl methacrylate
PSH	Phospholipids
ptDNA	Phosphorothioate DNA
QDs	Quantum dots
SAXS	Small-angle X-ray scattering
SERS	Surface enhanced Raman spectroscopy
SNA	Spherical nucleic acid
ssDNA	Single-stranded DNA
SSE	Single-stranded DNA encoders
SEM	Scanning electron microscope
TEM	Transmission electron microscope

## Conflicts of interest

There are no conflicts to declare.

## Acknowledgements

The authors are grateful for the financial support from the National Natural Science Foundation of China (22104087 and 22174093), the China Postdoctoral Science Foundation (2021M702107) and the Fundamental Research Funds for the Central Universities.

## References

- Z. Li, Q. Fan and Y. Yin, *Chem. Rev.*, 2022, **122**, 4976–5067.
- W. Li, H. Palis, R. Mérindol, J. Majimel, S. Ravaine and E. Duguet, *Chem. Soc. Rev.*, 2020, **49**, 1955–1976.
- S. C. Glotzer and M. J. Solomon, *Nat. Mater.*, 2007, **6**, 557–562.
- K. Deng, Z. Luo, L. Tan and Z. Quan, *Chem. Soc. Rev.*, 2020, **49**, 6002–6038.
- N. S. Mueller, Y. Okamura, B. G. M. Vieira, S. Juergensen, H. Lange, E. B. Barros, F. Schulz and S. Reich, *Nature*, 2020, **583**, 780–784.
- Y. Zhao, L. Shang, Y. Cheng and Z. Gu, *Accounts Chem. Res.*, 2014, **47**, 3632–3642.
- S. Wang, S. S. Park, C. T. Buru, H. Lin, P.-C. Chen, E. W. Roth, O. K. Farha and C. A. Mirkin, *Nat. Commun.*, 2020, **11**, 2495.
- R. Elghanian, J. J. Storhoff, R. C. Mucic, R. L. Letsinger and C. A. Mirkin, *Science*, 1997, **277**, 1078–1081.
- W. B. Rogers and V. N. Manoharan, *Science*, 2015, **347**, 639–642.
- Z. H. Ou, Z. W. Wang, B. B. Luo, E. Luijten and Q. Chen, *Nat. Mater.*, 2020, **19**, 450–455.
- E. Elacqua, X. Zheng, C. Shillingford, M. Liu and M. Weck, *Accounts Chem. Res.*, 2017, **50**, 2756–2766.
- L. H. Tan, H. Xing and Y. Lu, *Accounts Chem. Res.*, 2014, **47**, 1881–1890.
- M. R. Jones, N. C. Seeman and C. A. Mirkin, *Science*, 2015, **347**, 1260901.
- J. Li, A. A. Green, H. Yan and C. Fan, *Nat. Chem.*, 2017, **9**, 1056–1067.
- V. M. Prabhu and S. D. Hudson, *Nat. Mater.*, 2009, **8**, 365–366.
- C. A. Mirkin, R. L. Letsinger, R. C. Mucic and J. J. Storhoff, *Nature*, 1996, **382**, 607–609.
- Y. Wang, Y. Wang, D. R. Breed, V. N. Manoharan, L. Feng, A. D. Hollingsworth, M. Weck and D. J. Pine, *Nature*, 2012, **491**, 51–55.
- J. L. Banal, T. R. Shepherd, J. Berleant, H. Huang, M. Reyes, C. M. Ackerman, P. C. Blainey and M. Bathe, *Nat. Mater.*, 2021, **20**, 1272–1280.
- L. R. Hilliard, X. J. Zhao and W. H. Tan, *Anal. Chim. Acta*, 2002, **470**, 51–56.
- Y. Wang, Y. Wang, X. Zheng, É. Ducrot, J. S. Yodh, M. Weck and D. J. Pine, *Nat. Commun.*, 2015, **6**, 7253.
- S. Dey, C. Fan, K. V. Gothelf, J. Li, C. Lin, L. Liu, N. Liu, M. A. D. Nijenhuis, B. Saccà, F. C. Simmel, H. Yan and P. Zhan, *Nat. Rev. Methods Primers*, 2021, **1**, 13.
- A. P. Alivisatos, K. P. Johnsson, X. Peng, T. E. Wilson, C. J. Loweth, M. P. Bruchez, Jr. and P. G. Schultz, *Nature*, 1996, **382**, 609–611.
- J. I. Cutler, E. Auyeung and C. A. Mirkin, *J. Am. Chem. Soc.*, 2012, **134**, 1376–1391.
- D. Samanta, W. J. Zhou, S. B. Ebrahimi, S. H. Petrosko and C. A. Mirkin, *Adv. Mater.*, 2022, **34**, 2107875.
- W. B. Rogers, W. M. Shih and V. N. Manoharan, *Nat. Rev. Mater.*, 2016, **1**, 16008.
- C. L. Porter and J. C. Crocker, *Curr. Opin. Colloid In.*, 2017, **30**, 34–44.
- N. Liu and T. Liedl, *Chem. Rev.*, 2018, **118**, 3032–3053.
- J. S. Kahn, B. Minevich and O. Gang, *Curr. Opin. Biotech.*, 2020, **63**, 142–150.
- F. Li, J. Li, B. Dong, F. Wang, C. Fan and X. Zuo, *Chem. Soc. Rev.*, 2021, **50**, 5650–5667.
- T. Zhang, D. Lyu, W. Xu, Y. Mu and Y. Wang, *Front. Phys.*, 2021, **9**, 672375.

- 31 J. S. Kahn and O. Gang, *Angew. Chem., Int. Ed.*, 2022, **61**, e202105678.
- 32 S. Jiang, F. Zhang and H. Yan, *Nat. Mater.*, 2020, **19**, 694–700.
- 33 F. Hong, F. Zhang, Y. Liu and H. Yan, *Chem. Rev.*, 2017, **117**, 12584–12640.
- 34 L. Cademartiri and K. J. M. Bishop, *Nat. Mater.*, 2015, **14**, 2–9.
- 35 Y. Cui, J. C. Wang, J. C. Liang and H. B. Qiu, *Small*, 2023, **19**, 2207609.
- 36 T. Hueckel, G. M. Hocky and S. Sacanna, *Nat. Rev. Mater.*, 2021, **6**, 1053–1069.
- 37 X. N. Zhang, R. Wang and G. Xue, *Soft Matter*, 2015, **11**, 1862–1870.
- 38 N. Patra and A. V. Tkachenko, *Phys. Rev. E*, 2018, **98**, 032611.
- 39 J. D. Halverson and A. V. Tkachenko, *Phys. Rev. E*, 2013, **87**, 062310.
- 40 F. J. Rizzuto, T. Tuan and H. F. Sleiman, *Chem*, 2020, **6**, 1560–1574.
- 41 G. R. Yi, D. J. Pine and S. Sacanna, *J. Phys.: Condens. Matter*, 2013, **25**, 193101.
- 42 W. Liu, J. Halverson, Y. Tian, A. V. Tkachenko and O. Gang, *Nat. Chem.*, 2016, **8**, 867–873.
- 43 C. J. Loweth, W. B. Caldwell, X. G. Peng, A. P. Alivisatos and P. G. Schultz, *Angew. Chem., Int. Ed.*, 1999, **38**, 1808–1812.
- 44 S. A. Claridge, S. L. Goh, J. M. J. Fréchet, S. C. Williams, C. M. Micheel and A. P. Alivisatos, *Chem. Mater.*, 2005, **17**, 1628–1635.
- 45 Z. X. Deng, Y. Tian, S. H. Lee, A. E. Ribbe and C. D. Mao, *Angew. Chem., Int. Ed.*, 2005, **44**, 3582–3585.
- 46 X. Lan, Z. Chen, B. J. Liu, B. Ren, J. Henzie and Q. Wang, *Small*, 2013, **9**, 2308–2315.
- 47 D. Zanchet, C. M. Micheel, W. J. Parak, D. Gerion, S. C. Williams and A. P. Alivisatos, *J. Phys. Chem. B*, 2002, **106**, 11758–11763.
- 48 Z. Li, E. Cheng, W. Huang, T. Zhang, Z. Yang, D. Liu and Z. Tang, *J. Am. Chem. Soc.*, 2011, **133**, 15284–15287.
- 49 K.-M. Sung, D. W. Mosley, B. R. Peele, S. Zhang and J. M. Jacobson, *J. Am. Chem. Soc.*, 2004, **126**, 5064–5065.
- 50 J. Farlow, D. Seo, K. E. Broaders, M. J. Taylor, Z. J. Gartner and Y. W. Jun, *Nat. Methods*, 2013, **10**, 1203–1205.
- 51 G. Yao, H. Pei, J. Li, Y. Zhao, D. Zhu, Y. Zhang, Y. Lin, Q. Huang and C. Fan, *NPG Asia Mater.*, 2015, **7**, e159.
- 52 H. Xing, Y. G. Bai, Y. H. Bai, L. H. Tan, J. Tao, B. Pedretti, G. A. Vincil, Y. Lu and S. C. Zimmerman, *J. Am. Chem. Soc.*, 2017, **139**, 3623–3626.
- 53 J. Shen, Q. Tang, L. Li, J. Li, X. Zuo, X. Qu, H. Pei, L. Wang and C. Fan, *Angew. Chem., Int. Ed.*, 2017, **56**, 16077–16081.
- 54 G. B. Yao, J. Li, Q. Li, X. L. Chen, X. G. Liu, F. Wang, Z. B. Qu, Z. L. Ge, R. P. Narayanan, D. Williams, H. Pei, X. L. Zuo, L. H. Wang, H. Yan, B. Feringa and C. H. Fan, *Nat. Mater.*, 2020, **19**, 781–788.
- 55 M. Y. Ben Zion, X. He, C. C. Maass, R. Sha, N. C. Seeman and P. M. Chaikin, *Science*, 2017, **358**, 633–636.
- 56 Y. Ohya, N. Miyoshi, M. Hashizume, T. Tamaki, T. Uehara, S. Shingubara and A. Kuzuya, *Small*, 2012, **8**, 2335–2340.
- 57 H. Pei, F. Li, Y. Wan, M. Wei, H. Liu, Y. Su, N. Chen, Q. Huang and C. Fan, *J. Am. Chem. Soc.*, 2012, **134**, 11876–11879.
- 58 C. Chen, X. Wei, M. F. Parsons, J. Guo, J. L. Banal, Y. Zhao, M. N. Scott, G. S. Schlau-Cohen, R. Hernandez and M. Bathe, *Nat. Commun.*, 2022, **13**, 4935.
- 59 Y. Li, H. Lu, Z. Qu, M. Li, H. Zheng, P. Gu, J. Shi, J. Li, Q. Li, L. Wang, J. Chen, C. Fan and J. Shen, *Sci. China: Chem.*, 2022, **65**, 1212–1220.
- 60 G. Zhu, M. Hannel, R. Sha, F. Zhou, M. Y. Ben Zion, Y. Zhang, K. Bishop, D. Grier, N. Seeman and P. Chaikin, *Proc. Natl. Acad. Sci. U. S. A.*, 2021, **118**, e2023508118.
- 61 T. Zhang, Z. Q. Yang and D. S. Liu, *Nanoscale*, 2011, **3**, 4015–4021.
- 62 F. Huo, A. K. R. Lytton-Jean and C. A. Mirkin, *Adv. Mater.*, 2006, **18**, 2304–2306.
- 63 X. Xu, N. L. Rosi, Y. Wang, F. Huo and C. A. Mirkin, *J. Am. Chem. Soc.*, 2006, **128**, 9286–9287.
- 64 K. Suzuki, K. Hosokawa and M. Maeda, *J. Am. Chem. Soc.*, 2009, **131**, 7518–7519.
- 65 T. Zhang, Y. Dong, Y. Sun, P. Chen, Y. Yang, C. Zhou, L. Xu, Z. Yang and D. Liu, *Langmuir*, 2012, **28**, 1966–1970.
- 66 T. G. W. Edwardson, K. L. Lau, D. Bousmail, C. J. Serpell and H. F. Sleiman, *Nat. Chem.*, 2016, **8**, 162–170.
- 67 T. Tuan, C. Liao, V. Toader, M. Barlog, H. S. Bazzi, J. Li and H. F. Sleiman, *Nat. Chem.*, 2018, **10**, 184–192.
- 68 N. L. Xie, S. Y. Liu, H. M. Fang, Y. J. Yang, K. Quan, J. Li, X. H. Yang, K. M. Wang and J. Huang, *ACS Nano*, 2019, **13**, 4174–4182.
- 69 R. J. Niu, C. Y. Song, F. Gao, W. N. Fang, X. Y. Jiang, S. K. Ren, D. Zhu, S. Su, J. Chao, S. F. Chen, C. H. Fan and L. H. Wang, *Angew. Chem., Int. Ed.*, 2021, **60**, 11695–11701.
- 70 Y. Xiong, S. Yang, Y. Tian, A. Michelson, S. Xiang, H. Xin and O. Gang, *ACS Nano*, 2020, **14**, 6823–6833.
- 71 Y. Zhang, J. Chao, H. Liu, F. Wang, S. Su, B. Liu, L. Zhang, J. Shi, L. Wang, W. Huang, L. Wang and C. Fan, *Angew. Chem., Int. Ed.*, 2016, **55**, 8036–8040.
- 72 B. Liu, C. Song, D. Zhu, X. Wang, M. Zhao, Y. Yang, Y. Zhang, S. Su, J. Shi, J. Chao, H. Liu, Y. Zhao, C. Fan and L. Wang, *Small*, 2017, **13**, 1603991.
- 73 X. Chen, X. Liu, G. Yao, Q. Li, R. Liu, H. Wu, Y. Lv, C. Fan, L. Wang and J. Li, *NPG Asia Mater.*, 2020, **12**, 49.
- 74 L. G. Xu, H. Kuang, C. L. Xu, W. Ma, L. B. Wang and N. A. Kotov, *J. Am. Chem. Soc.*, 2012, **134**, 1699–1709.
- 75 W. Ma, H. Kuang, L. Xu, L. Ding, C. Xu, L. Wang and N. A. Kotov, *Nat. Commun.*, 2013, **4**, 2689.
- 76 D. Zhao, Z. L. Zhang, Y. Q. Wen, X. J. Zhang and Y. L. Song, *Appl. Phys. Lett.*, 2013, **102**, 123101.
- 77 G. Q. Wang, Y. Akiyama, N. Kanayama, T. Takarada and M. Maeda, *Small*, 2017, **13**, 1702137.
- 78 J. E. Millstone, D. G. Georganopoulos, X. Y. Xu, W. Wei, S. Y. Li and C. A. Mirkin, *Small*, 2008, **4**, 2176–2180.
- 79 G. Wang, Y. Zhang, X. Liang, T. Takarada and M. Maeda, *Nanomaterials*, 2019, **9**, 581.
- 80 W. Ren, Y. Zhou, S. Wen, H. He, G. Lin, D. Liu and D. Jin, *Chem. Commun.*, 2018, **54**, 7183–7186.

- 81 E. E. Coughlin, J. T. Hu, A. Lee and T. W. Odom, *J. Am. Chem. Soc.*, 2021, **143**, 3671–3676.
- 82 F. Lu, V. Thi, Y. Zhang, A. Frenkel, K. G. Yager, S. Kumar and O. Gang, *Sci. Adv.*, 2019, **5**, eaaw2399.
- 83 J. Wang, L. Hu, Y. Song and M. J. Serpe, *Polymer*, 2014, **55**, 2340–2346.
- 84 W. Xu, M. Wei and M. J. Serpe, *Adv. Opt. Mater.*, 2017, **5**, 1600614.
- 85 Y. Zhou, Y. Yang, X. Deng, G. Zhang, Y. Zhang, C. Zhang, S. Shuang, Y. He and W. Sun, *Sensor. Actuat. B-Chem.*, 2018, **276**, 204–210.
- 86 E. Chowdhury, C. A. Grapperhaus and M. G. O'Toole, *J. Nanopart. Res.*, 2020, **22**, 142.
- 87 M. M. Maye, D. Nykypanchuk, M. Cuisinier, D. van der Lelie and O. Gang, *Nat. Mater.*, 2009, **8**, 388–391.
- 88 W. W. Qin, T. H. Peng, Y. J. Gao, F. Wang, X. C. Hu, K. Wang, J. Y. Shi, D. Li, J. C. Ren and C. H. Fan, *Angew. Chem., Int. Ed.*, 2017, **56**, 515–518.
- 89 L. Feng, L. L. Pontani, R. Dreyfus, P. Chaikin and J. Brujic, *Soft Matter*, 2013, **9**, 9816–9823.
- 90 Q. Y. Lin, J. A. Mason, Z. Y. Li, W. J. Zhou, M. N. O'Brien, K. A. Brown, M. R. Jones, S. Butun, B. Lee, V. P. Dravid, K. Aydin and C. A. Mirkin, *Science*, 2018, **359**, 669–672.
- 91 L. Feng, R. Dreyfus, R. Sha, N. C. Seeman and P. M. Chaikin, *Adv. Mater.*, 2013, **25**, 2779–2783.
- 92 L. H. Tan, H. Xing, H. Chen and Y. Lu, *J. Am. Chem. Soc.*, 2013, **135**, 17675–17678.
- 93 G. Chen, K. J. Gibson, D. Liu, H. C. Rees, J. H. Lee, W. W. Xia, R. Q. Lin, H. L. L. Xin, O. Gang and Y. Weizmann, *Nat. Mater.*, 2019, **18**, 169–174.
- 94 J. Moon, I.-S. Jo, E. Ducrot, J. S. Oh, D. J. Pine and G.-R. Yi, *Macromol. Res.*, 2018, **26**, 1085–1094.
- 95 M. R. Jones and C. A. Mirkin, *Nature*, 2012, **491**, 42–43.
- 96 J. S. Oh, S. Lee, S. C. Glotzer, G.-R. Yi and D. J. Pine, *Nat. Commun.*, 2019, **10**, 3936.
- 97 M. Z. Liu, X. L. Zheng, V. Grebe, M. X. He, D. J. Pine and M. Weck, *Angew. Chem., Int. Ed.*, 2021, **60**, 5744–5748.
- 98 X. Zheng, Y. Wang, Y. Wang, D. J. Pine and M. Weck, *Chem. Mater.*, 2016, **28**, 3984–3989.
- 99 J. S. Oh, G.-R. Yi and D. J. Pine, *ACS Nano*, 2020, **14**, 15786–15792.
- 100 M. He, J. P. Gales, X. Shen, M. J. Kim and D. J. Pine, *Langmuir*, 2021, **37**, 7246–7253.
- 101 M. He, J. P. Gales, É. Ducrot, Z. Gong, G.-R. Yi, S. Sacanna and D. J. Pine, *Nature*, 2020, **585**, 524–529.
- 102 J. A. Diaz A, J. S. Oh, G.-R. Yi and D. J. Pine, *Proc. Natl. Acad. Sci. U. S. A.*, 2020, **117**, 10645–10653.
- 103 D. Morphew, J. Shaw, C. Avins and D. Chakrabarti, *ACS Nano*, 2018, **12**, 2355–2364.
- 104 A. Neophytou, V. N. Manoharan and D. Chakrabarti, *ACS Nano*, 2021, **15**, 2668–2678.
- 105 N. C. Seeman, *J. Theor. Biol.*, 1982, **99**, 237–247.
- 106 P. W. K. Rothemund, *Nature*, 2006, **440**, 297–302.
- 107 Z. Ge, H. Gu, Q. Li and C. Fan, *J. Am. Chem. Soc.*, 2018, **140**, 17808–17819.
- 108 Z. Zhao, E. L. Jacovetty, Y. Liu and H. Yan, *Angew. Chem., Int. Ed.*, 2011, **50**, 2041–2044.
- 109 X. Luo, P. Chidchob, J. F. Rahbani and H. F. Sleiman, *Small*, 2018, **14**, 1702660.
- 110 C. Zhang, X. Li, C. Tian, G. Yu, Y. Li, W. Jiang and C. Mao, *ACS Nano*, 2014, **8**, 1130–1135.
- 111 Y. Li, Z. Liu, G. Yu, W. Jiang and C. Mao, *J. Am. Chem. Soc.*, 2015, **137**, 4320–4323.
- 112 C. Shen, X. Lan, X. Lu, T. A. Meyer, W. Ni, Y. Ke and Q. Wang, *J. Am. Chem. Soc.*, 2016, **138**, 1764–1767.
- 113 R. Schreiber, I. Santiago, A. Ardavan and A. J. Turberfield, *ACS Nano*, 2016, **10**, 7303–7306.
- 114 Y. Tian, J. R. Lhermitte, L. Bai, T. Vo, H. L. L. Xin, H. L. Li, R. P. Li, M. Fukuto, K. G. Yager, J. S. Kahn, Y. Xiong, B. Minevich, S. K. Kumar and O. Gang, *Nat. Mater.*, 2020, **19**, 789–796.
- 115 W. Y. Liu, M. Tagawa, H. L. L. Xin, T. Wang, H. Emamy, H. L. Li, K. G. Yager, F. W. Starr, A. V. Tkachenko and O. Gang, *Science*, 2016, **351**, 582–586.
- 116 V. Linko and M. A. Kostiainen, *Nat. Mater.*, 2020, **19**, 706–707.
- 117 Y. Dong, J. Liu, X. Lu, J. Duan, L. Zhou, L. Dai, M. Ji, N. Ma, Y. Wang, P. Wang, J. J. Zhu, Q. Min, O. Gang and Y. Tian, *Nano Lett.*, 2022, **22**, 3809–3817.
- 118 Y. Zhou, J. Dong, C. Zhou and Q. Wang, *Angew. Chem., Int. Ed.*, 2022, e202116416.
- 119 M. Ji, J. Liu, L. Dai, L. Wang and Y. Tian, *J. Am. Chem. Soc.*, 2020, **142**, 21336–21343.
- 120 Z. Lin, H. Emamy, B. Minevich, Y. Xiong, S. Xiang, S. Kumar, Y. Ke and O. Gang, *J. Am. Chem. Soc.*, 2020, **142**, 17531–17542.
- 121 L. Shani, A. N. Michelson, B. Minevich, Y. Fleger, M. Stern, A. Shaulov, Y. Yeshurun and O. Gang, *Nat. Commun.*, 2020, **11**, 5697.
- 122 M. Y. Wang, L. Z. Dai, J. L. Duan, Z. Y. Ding, P. Wang, Z. Li, H. Xing and Y. Tian, *Angew. Chem., Int. Ed.*, 2020, **59**, 6389–6396.
- 123 Y. Wang, X. Yan, Z. Zhou, N. Ma and Y. Tian, *Angew. Chem., Int. Ed.*, 2022, **61**, e202208290.
- 124 X. Yan, Y. Wang, N. Ma, Y. Yu, L. Dai and Y. Tian, *J. Am. Chem. Soc.*, 2023, **145**, 3978–3986.
- 125 M. Ji, Z. Zhou, W. Cao, N. Ma, W. Xu and Y. Tian, *Sci. Adv.*, 2022, **8**, eadc9755.
- 126 C. M. Wintersinger, D. Minev, A. Ershova, H. M. Sasaki, G. Gowri, J. F. Berengut, F. E. Corea-Dilbert, P. Yin and W. M. Shih, *Nat. Nanotech.*, 2023, **18**, 281–289.
- 127 G. Yao, F. Zhang, F. Wang, T. Peng, H. Liu, E. Poppletton, P. Šulc, S. Jiang, L. Liu, C. Gong, X. Jing, X. Liu, L. Wang, Y. Liu, C. Fan and H. Yan, *Nat. Chem.*, 2020, **12**, 1067–1075.
- 128 X. Chen, Y. Wang, X. Dai, L. Ding, J. Chen, G. Yao, X. Liu, S. Luo, J. Shi, L. Wang, R. Nechushtai, E. Pikarsky, I. Willner, C. Fan and J. Li, *J. Am. Chem. Soc.*, 2022, **144**, 6311–6320.
- 129 S. Sun, S. Yang, H. L. Xin, D. Nykypanchuk, M. Liu, H. Zhang and O. Gang, *Nat. Commun.*, 2020, **11**, 2279.

- 130 A. Michelson, B. Minevich, H. Emamy, X. Huang, Y. S. Chu, H. Yan and O. Gang, *Science*, 2022, **376**, 203–207.
- 131 S. Jia, J. Wang, M. Xie, J. Sun, H. Liu, Y. Zhang, J. Chao, J. Li, L. Wang, J. Lin, K. V. Gothelf and C. Fan, *Nat. Commun.*, 2019, **10**, 5597.
- 132 X. Dai, X. Chen, X. Jing, Y. Zhang, M. Pan, M. Li, Q. Li, P. Liu, C. Fan and X. Liu, *Angew. Chem., Int. Ed.*, 2022, **61**, e202114190.
- 133 E. Braun, Y. Eichen, U. Sivan and G. Ben-Yoseph, *Nature*, 1998, **391**, 775–778.
- 134 Y. X. Shang, N. Li, S. B. Liu, L. Wang, Z. G. Wang, Z. Zhang and B. Q. Ding, *Adv. Mater.*, 2020, **32**, 2000294.
- 135 Y. Zhao, C. Zhang, L. Yang, X. Xu, R. Xu, Q. Ma, Q. Tang, Y. Yang and D. Han, *Small*, 2021, **17**, 2103877.
- 136 Z. G. Wang, Q. Liu and B. Q. Ding, *Chem. Mater.*, 2014, **26**, 3364–3367.
- 137 X. G. Liu, F. Zhang, X. X. Jing, M. C. Pan, P. Liu, W. Li, B. W. Zhu, J. Li, H. Chen, L. H. Wang, J. P. Lin, Y. Liu, D. Y. Zhao, H. Yan and C. H. Fan, *Nature*, 2018, **559**, 593–598.
- 138 X. X. Jing, F. Zhang, M. C. Pan, X. P. Dai, J. Li, L. H. Wang, X. G. Liu, H. Yan and C. H. Fan, *Nat. Protoc.*, 2019, **14**, 2416–2436.
- 139 Y. Wang, L. Dai, Z. Ding, M. Ji, J. Liu, H. Xing, X. Liu, Y. Ke, C. Fan, P. Wang and Y. Tian, *Nat. Commun.*, 2021, **12**, 3011.
- 140 L. Liang, P. Zheng, C. Zhang and I. Barman, *Adv. Mater.*, 2021, **33**, 2005133.